"Enabling Technologies for Ceramic Hot Section Components"

Performed under Department of Energy Interagency Agreement DE-AI26-03CH11142

with the Office of Naval Research (ONR) Contracts N00014-03-C-0477 (Volume 1) and N00014-06-C-0585(Volume 2)

Program Managers

Venkat Vedula
Tania Bhatia

United Technologies Research Center
M/S 129-88
411 Silver Lane
East Hartford, Connecticut 60108

April, 2009

DISCLAIMER

Executive Summary

Silicon-based ceramics are attractive materials for use in gas turbine engine hot sections due to their high temperature mechanical and physical properties as well as lower density than metals. The advantages of utilizing ceramic hot section components include weight reduction, and improved efficiency as well as enhanced power output and lower emissions as a result of reducing or eliminating cooling. Potential gas turbine ceramic components for industrial, commercial and/or military high temperature turbine applications include combustor liners, vanes, rotors, and shrouds. These components require materials that can withstand high temperatures and pressures for long duration under steam-rich environments.

For Navy applications, ceramic hot section components have the potential to increase the operation range. The amount of weight reduced by utilizing a lighter gas turbine can be used to increase fuel storage capacity while a more efficient gas turbine consumes less fuel. Both improvements enable a longer operation range for Navy ships and aircraft. Ceramic hot section components will also be beneficial to the Navy's Growth Joint Strike Fighter (JSF) and VAATE (Versatile Affordable Advanced Turbine Engines) initiatives in terms of reduced weight, cooling air savings, and capability/cost index (CCI).

For DOE applications, ceramic hot section components provide an avenue to achieve low emissions while improving efficiency. Combustors made of ceramic material can withstand higher wall temperatures and require less cooling air. Ability of the ceramics to withstand high temperatures enables novel combustor designs that have reduced NO_x, smoke and CO levels. In the turbine section, ceramic vanes and blades do not require sophisticated cooling schemes currently used for metal components. The saved cooling air could be used to further improve efficiency and power output.

The objectives of this contract were to develop technologies critical for ceramic hot section components for gas turbine engines. Significant technical progress has been made towards maturation of the EBC and CMC technologies for incorporation into gas turbine engine hot-section. Promising EBC candidates for longer life and/or higher temperature applications relative to current state of the art BSAS-based EBCs have been identified. These next generation coating systems have been scaled-up from coupons to components and are currently being field tested in Solar Centaur 50S engine. CMC combustor liners were designed, fabricated and tested in a FT8 sector rig to demonstrate the benefits of a high temperature material system. Pretest predictions made through the use of perfectly stirred reactor models showed a 2-3x benefit in CO emissions for CMC versus metallic liners. The sector-rig test validated the pretest predictions with >2x benefit in CO at the same NOx levels at various load conditions. The CMC liners also survived several trip shut downs thereby validating the CMC design methodology.

Significant technical progress has been made towards incorporation of ceramic matrix composites (CMC) and environmental barrier coatings (EBC) technologies into gas turbine engine hot-section. The second phase of the program focused on the demonstration of a reverse flow annular CMC combustor. This has included overcoming

the challenges of design and fabrication of CMCs into “complex” shapes; developing processing to apply EBCs to “engine hardware”; testing of an advanced combustor enabled by CMCs in a PW206 rig; and the validation of performance benefits against a metal baseline. The rig test validated many of the pretest predictions with a 40-50% reduction in pattern factor compared to the baseline and reductions in NOx levels at maximum power conditions. The next steps are to develop an understanding of the life limiting mechanisms in EBC and CMC materials, developing a design system for EBC coated CMCs and durability testing in an engine environment.

Final Contract Report
Office of Naval Research N00014-03-C-0477

"Enabling Technologies for Ceramic Hot Section Components"
VOLUME 1

Venkat Vedula
Program Manager

United Technologies Research Center
M/S 129-88
411 Silver Lane
East Hartford, Connecticut 60108

October 9, 2006

TABLE OF CONTENTS

LIST OF FIGURES

LIST OF TABLES

1. Environmental Barrier Coatings (EBC) for Silicon-based Ceramics

1.1 Background

In 1949 and 1951, A.C. Lea[1] studied and reported on the rate of oxidation of silicon carbide and noted that steam caused the oxidation rate to be accelerated compared to the rate in dry oxygen. The volatilization of silica in an air-steam atmosphere was presented as a possible mechanism to explain the observation. Almost 50 years later, Opila and Hann[2], Opila, Fox, and Jacobson[3], and Opila, Smialek, Robinson, Fox, and Jacobson[4] studied in detail and presented a model explaining the accelerated oxidation of silicon carbide due to high temperature exposure to steam. Their work showed that, on exposure to steam, oxidation of silicon carbide occurs by a paralinear rate process involving oxidation of silicon carbide by H_2O to form silica and then volatilization of the silica by reaction with H_2O to form Si-O-H(g) species (see equations 1 & 2). For overall paralinear behavior, the silica layer that forms on the substrate due to oxidation occurs by a parabolic rate process while the volatilization of the silica occurs by a linear rate process. Over long times the growth rate process of silica formation is balanced by the volatilization process at which time further oxidation of the substrate is controlled simply by the linear volatilization rate. The silica scale reaches a steady state thickness of approximately 10 microns for temperatures in the range of 1200°C to 1400°C (2200°F to 2550°F). This is contrasted with oxidation under dry conditions, whereby oxidation is governed by a parabolic rate process involving the formation and growth of a stable, protective silica scale on the surface of silicon carbide.

$$(1) \qquad SiC + 3H_2O_{(g)} = SiO_2 + 3H_{2(g)} + CO_{(g)}$$

$$(2) \qquad SiO_2 + H_2O_{(g)} = Si\text{-}O_x\text{-}H_{y(g)}$$

Further work by these authors modeled the volatilization process and showed that the flux of the volatile species is controlled by diffusion through a boundary layer. For a flat plate geometry and for laminar flow, the flux is predicted to be dependent on the gas velocity and pressures as shown in equation (3) for when the volatile silicon species is $Si(OH)_4$ which is the predicted dominant species for fuel lean, gas turbine combustion environments.

$$(3) \qquad J_{Si(OH)4} \propto v^{1/2} \cdot (P_{H2O})^2 / (P_{total})^{1/2}$$

where J is the flux, v is the gas velocity and P is either the total system pressure or partial pressure of steam.

Experimental work by Robinson and Smialek[5] in a high-pressure combustion test facility measured SiC recession versus test conditions and confirmed equation (3) for lean combustion conditions. Figure 1 summarizes the results for lean burn conditions over the temperature range of approximately 1200°C to 1450°C (2200°F to 2650°F). Table 1 provides predictions based on the experimental data for long-term recession of SiC in a combustion environment. The predicted recession at 1200°C (2200°F) of 270 microns in 1000 hours in a combustion environment for SiC is too significant to ignore for a material with expected useful life 30,000 hours in a proposed application such as an industrial gas

turbine. Confirmation of this behavior in actual engine environments has been observed in a Solar Turbines, Inc. Centaur 50S industrial gas turbine[6]. The Solar Turbines, Inc. engine was run with SiC CMC combustor liners at nominally 1200°C (2200°F) for 5,018 hours. Recession values of up to ~2200 microns were measured. This recession rate is roughly 0.44 microns per hour to result in a 1,000 hour calculated recession of 440 microns, which is similar to the predicted loss of 270 microns in 1,000 hours at 1200°C (2200°F) from Table 1. Figure 2 is a view of the liner in cross section at two different locations after 5,108 hours.

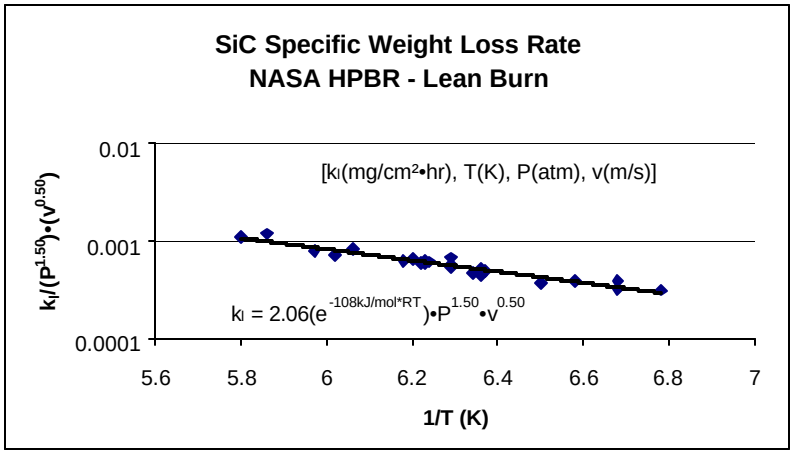

Figure 1: Experimental recession measurements of SiC in a high-pressure combustion environment.

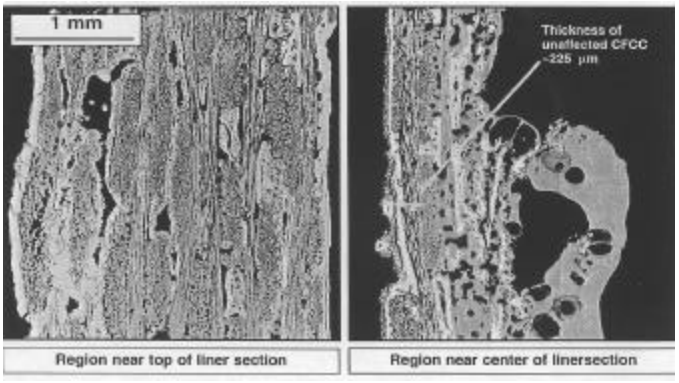

Figure 2: Cross sectional view of Solar Turbines, Inc SiC CMC Centaur 50S combustor liner after 5,018 hrs operation @ nominally 1200°C showed more than 90% oxidation.

Table 1: Predicted recession of SiC under lean burn combustion conditions (Ref. 5).

T (°C)	Predicted Lean Burn Recession (μm) 1000 hrs, 10 atm, 90 m/s
1000	70
1100	140
1200	270
1300	480
1400	790
1500	1230

1.2 EBC Development for SiC/SiC CMCs

Lessons Learned from Post-Test Analysis of BSAS EBC-Coated CMC Combustor Liners

The current state-of-the-art 3-layer Barium Strontium Aluminum Silicate (BSAS) based EBCs have been demonstrated for more than 50,000 hours cumulative (15,144 hours continuous) at nominal 1200°C (~2200°F) in Solar Turbines Centaur 50S engine tests, under the Ceramic Stationary Gas Turbine (CSGT) and Advanced Material Program sponsored by the U.S. Department of Energy (DoE). Engine tests have been performed at two sites: ChevronTexaco Exploration and Production Inc. in Bakersfield, CA and Malden Mills Industries in Lawrence, MA. To date, eight sets of combustor liners with BSAS-based EBCs applied by UTRC have been tested. The lessons learnt from these engine tests have laid the foundation for continued improvements in the EBC coatings and develop a fundamental understanding of the life limiting mechanisms.

The primary observation made on most of the long-term engine tests (~14,000 hrs and more) was the extensive thinning of BSAS top layer. This was exemplified in the mid-section (presumably exposed to the highest temperature) of the combustor liners where the fuel injectors were located. Figure 3 below shows extensive thinning of the BSAS top layer after 13,937-hour engine test at the Bakersfield site. The polished cross-section shows that the thickness of the BSAS top layer decreased from 125 μm at the start of the test to less than 30 μm after the test.

One of the objectives in development of next generation EBCs is to develop coatings for 1315°C (2400°F) applications and to extend the life at 1200°C (~2200°F) beyond 15,000 hours. A strategy to achieve this objective was to identify alternate top layer compositions that were more stable in high temperature steam environment than BSAS. Strontium Aluminum Silicate (SAS) and Yttrium Silicate (YS) have been previously identified as potential candidates.

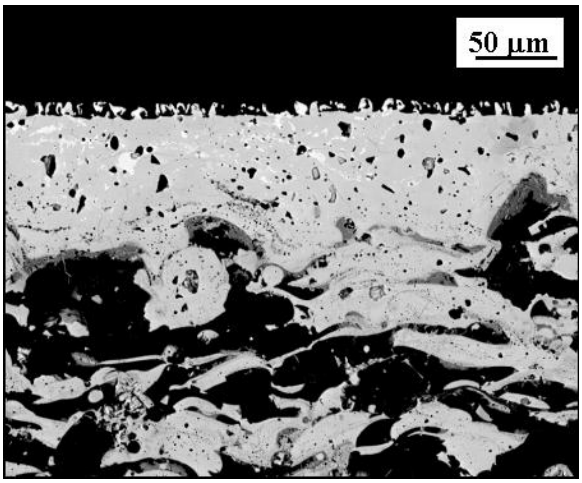

Figure 3: BSAS-based EBC after 13,937 hours of engine field test.

Lessons Learned from Engine Testing of SAS Coatings

SAS based EBC's were field tested in Solar Turbines Centaur 50S engine (Malden Mills 3) and had completed 8,368 hours with 32 starts and stops. In this engine test, the outer CMC combustor liner was coated with a 3-layer EBC system (SAS / SAS + Mullite / Si) whereas the inner liner was coated with a 2-layer EBC system (SAS / Si). Figure 4 below shows the coated liners after the engine field test. The 3-layer SAS coating appeared pristine with no visible EBC degradation or spallation whereas the 2-layer EBC system showed significant spallation. In the latter case, the spallation is linked to non-optimized processing of the SAS coating. Since the coatings were first developed and applied to these liners, significant process improvements have been made to improve the quality of the coatings.

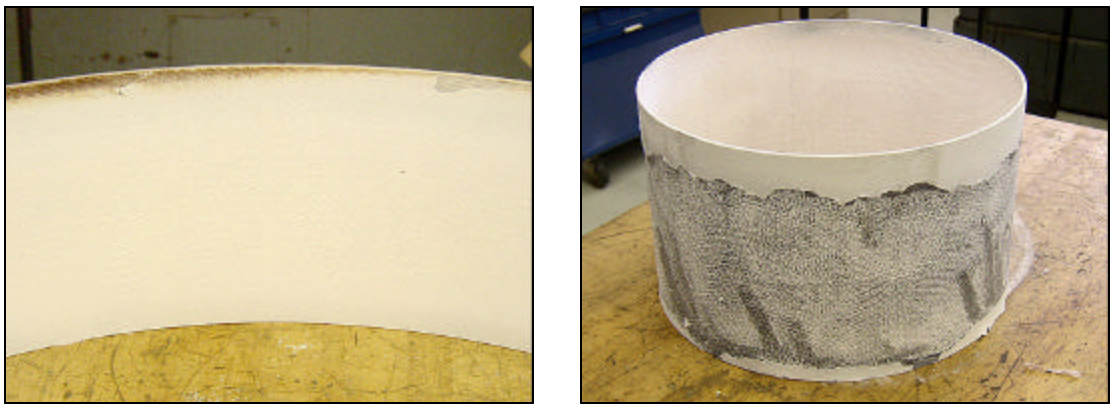

Figure 4: Solar Turbines Centaur 50S Combustor Liners: Outer liner with 3-layer SAS based EBC (left) and inner liner with 2-layer EBC (right) after 8,368 hours of field test.

The post-test analyses of SAS based EBCs from inner and outer liners provided key insights into EBC recession and coating life. Detailed microstructural evaluation of the aft end of inner liner indicated minimal SAS recession and the formation of silica (25 to 50 μm thick) between silicon bond coat and SAS top layer. In addition, extensive amount of porosity was also observed in the SAS layer, especially close to the Si/SAS interface. The most likely reason for EBC spallation was the coalescing of voids present along the Si/SAS interface. A Sr-rich and silicon depleted phase was detected in the gas path surface of the SAS top coat following the engine test. It is presumed that the silica present in SAS matrix volatilized during the engine test leaving behind a Sr-rich phase. The backside of the CMC combustor liners was not coated with silicon carbide seal coat in order to reduce cost. It was found that the unprotected backside of the liners were attacked by the exhaust gas causing significant oxidation and ~1.5 mm thick silica scale was observed in several regions. The analysis also showed preferential oxidation of silicon matrix within the CMC, indicating poor infiltration of melt silicon during the MI SiC/SiC processing.

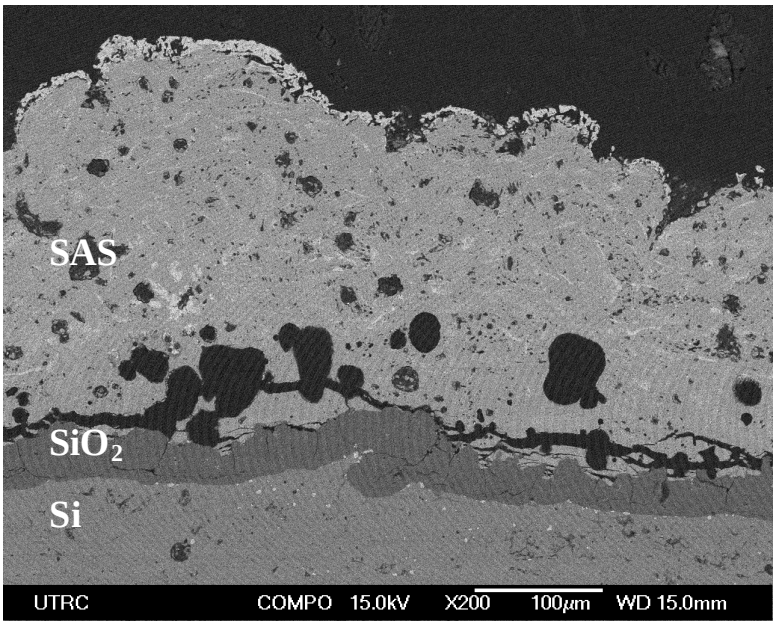

Figure 5: Aft end of inner liner showing silica formation at Si/SAS interface and coalescing of voids along the interface

The EBC coated outer liners looked pristine visually after the engine field test. However, detailed microstructural analysis revealed that the SAS top coat was lost leaving a layer of secondary $Sr_2Al_2SiO_7$ phase. This secondary phase was found on the mixed intermediate layer (SAS + Mullite). Quantification of the amount of "recession" in the SAS top layer on the outer liner could not be made because of an absence of the corresponding witness coupons. In majority of the areas, the mixed layer was intact but it did not appear to offer any protection to the CMC substrate. A thick silica layer was formed between the intermediate layer and silicon bond coat and in several areas the entire silicon was consumed and attack on CMC was observed.

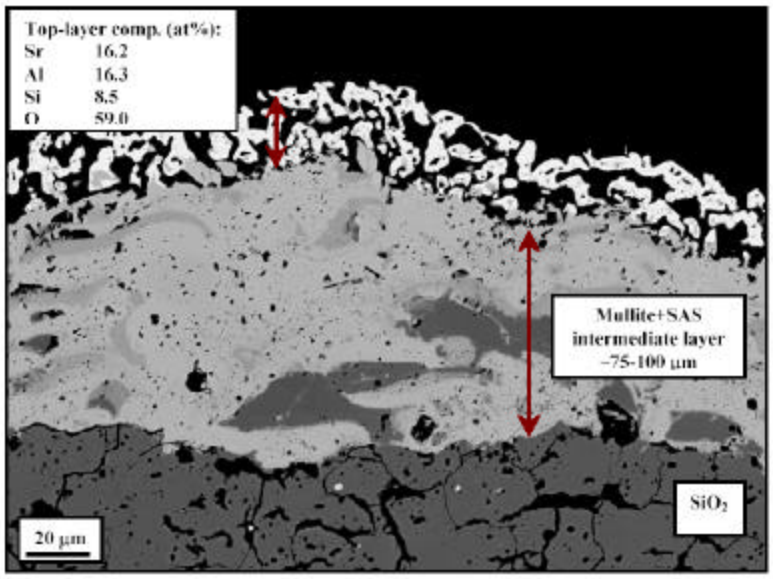

Figure 6: Outer liner after 8,368-hour engine testing showing loss of SAS top coat

In summary, SAS based EBC coated liners demonstrated less than expected results due to processing related issues. As reported previously, significant improvements in the SAS coating quality have been made and the improved coatings are projected to have life of 15,000 hours or higher under Centaur 50S like conditions. The MM-3 engine test also demonstrated that SAS is inherently more stable than BSAS. There were no eutectic phases detected between SAS and silicon and minimal recession of intermediate layer was observed after the field test.

Coating of Solar Liners for Field Testing

After learning the importance of well processed coatings, a significant effort was focused on improving the quality of coatings of the compositions expected to extend the recession life of the coated CMC in a Solar Engine field test. UTRC successfully coated a set of combustor liners that are currently being engine field tested at California Dairies site in Visalia, CA. The inner liner was coated with Si/mullite/SAS multi-layer coating and the outer liner was coated with 2-layer Si/yttrium silicate EBC. The typical microstructures of the inner and outer liners are shown below.

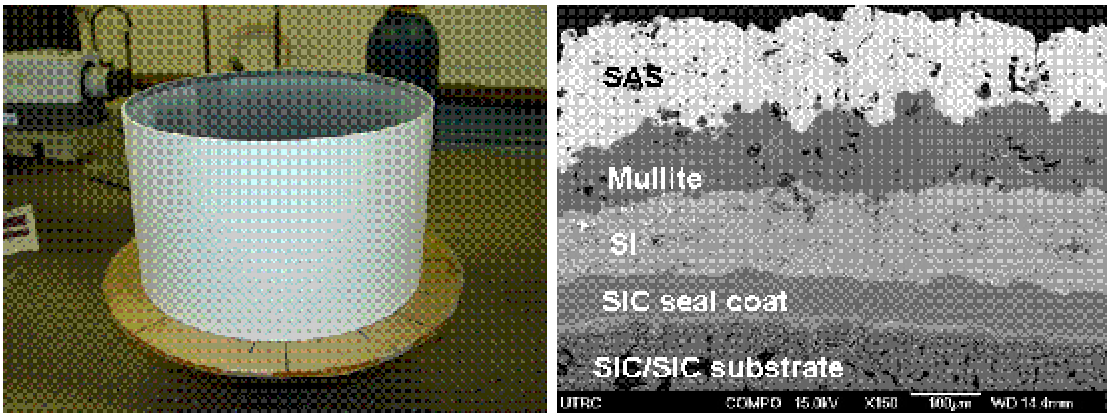

(a) Solar inner liner with SAS coating

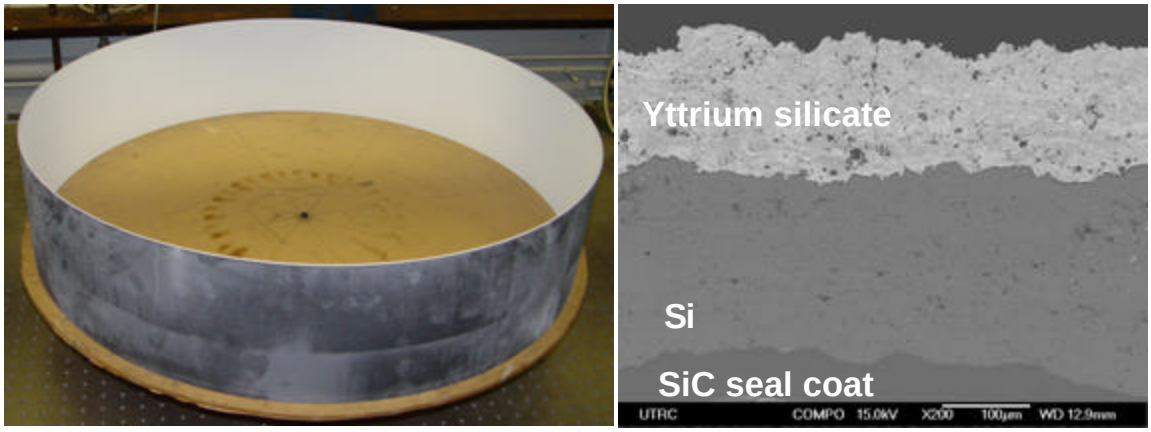

(b) Solar Outer Liner with Yttrium silicate coating

Figure 7: EBC coated Solar Centaur 50S CMC combustor liners

EBC Life Prediction

To facilitate the use of EBC coated ceramics across the next generation of ceramic products, it is important to understand and predict the failure modes in these materials. The various causes of coating failure have been identified to be (i) Coating recession, (ii) Bond coat oxidation and thermally grown oxide (TGO) growth, (iii) Mechanical degradation of substrate due to coating, (iv) Erosion, (v) Foreign Object Damage (FOD) (vi) Hot corrosion and (vii) Creep. Figure 3 is an example of coating recession and Figure 8 shows bond coat oxidation in BSAS-based EBC on SiC/SiC CMC after ~14,000 hours in engine field test. A major technology gap exists in the understanding of most of the above identified failure modes. Also, there is a gap in understanding the various conditions under which particular mode(s) determines component life. The first step towards developing life prediction maps is to develop validated models for the different life limiting mechanisms.

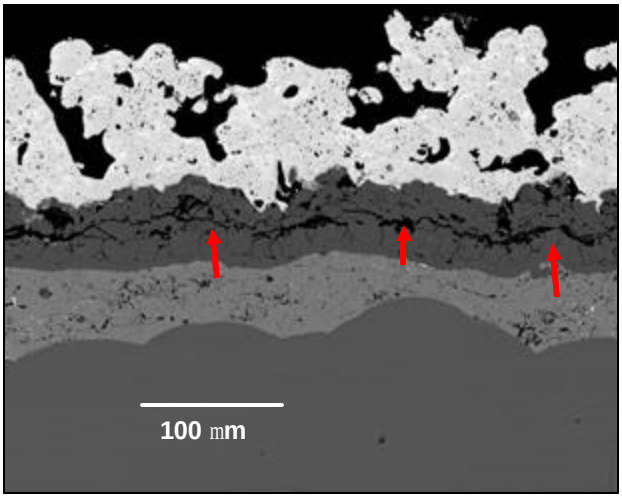

Figure 8: Failure of EBC after 13,937 hrs of engine field testing. Spallation consistently occurs at SiO2/mullite interface and at processing defects, and geometric imperfections of CMC

Initial calculations were performed to estimate the recession of BSAS and SAS coating on a combustor in a FT8 like operating environment. For the purpose of these calculations, the combustor wall temperature was set at 2200°F (1204°C). In trying to generate these calculations, a number of simplifications had to be made because the thermodynamic data for many of the potential phases (degradation products of SAS, BSAS and BAS) does not exist. The rate of loss of BSAS in the combustor operating in the Solar engine had been found to be ~9 microns/1000 hours. This is equivalent to 8.9 mils/25000 hours. The relevant reactions considered are:

(4) SrO*Al2O3*2SiO2 ----> SrAl2O4 + 2SiO2
(5) BaO*Al2O3*2SiO2 ----> BaAl2O4 + 2SiO2
(6) 2SiO2 + 4H2O(g) ----> Si(OH)4(g)
(7) SrO*Al2O3*2SiO2 + 4H2O(g) -----> SrAl2O4 + 4Si(OH)4(g).
(8) BaO*Al2O3*2SiO2 + 4H2O(g) -----> BaAl2O4 + 4Si(OH)4(g).

Based on the enthalpies of reaction available for the above reactions, and the assumption that the primary mechanism of recession is the leaching of SiO_2, calculations were performed to predict the difference in projected life times under Solar and FT8 conditions which are summarized in Table 2 below.

Table 2: Prediction of recession of SAS and BSAS coatings using simple recession models based on SiO_2 activity.

Engine	**mils of coating loss/25000 hours**		
	SAS	BSAS	BAS
Solar	2	9	15
FT8	8	31	51

A significant reason for the higher calculated loss rate in the FT8 engine as compared with the Solar Turbines' engine is the increased partial pressure of water vapor, i.e. 3.45 atmospheres vs. 1 atmosphere. Further work is required in order to validate that the SiO_2 activity controls the overall recession of the complex silicates to determine the actual recession mechanisms and to refine the predictive modeling capability.

1.3 EBC Development for Silicon Nitride

Emphasis on the development of non-line-of-sight coatings

As efforts got underway to develop a coating system for monolithic Si_3N_4, the complexity and small size of the components that needed to be coated were considered in the planning phase of the program. Most of the prior experience in EBC development to date consisted of plasma sprayed coatings and it appeared that existing thermal spray technologies might not be suitable to coat the components of interest. A detailed feasibility study was performed to determine if an air plasma spray technique can be used to coat complex shaped engine components such as integral vane rings and integrally bladed rotors (IBR). The feasibility study was based on a simple analytical approach that considered the ability of a plasma gun to coat "hidden" areas (vanes and platforms) by calculating the angle at which the spray gun approached the component without "gouging". The ST5+ vane ring that was previously designed and fabricated under the DoE Advanced Microturbine contract was used for the plasma spray feasibility assessment. The approach is illustrated in Figure 9. The quality of coating as a function of gun-angle was independently assessed by thermal spraying a cylinder. The other factors that were considered in the final feasibility assessment included fixtures, cost, coating uniformity and existing mini-gun technologies. It was established that air plasma spray could not be used to apply acceptable quality environmental barrier coatings (EBCs) to an integral vane ring assembly. It was determined that chemical vapor deposition (CVD) and/or slurry based non-line-of-sight approaches (such as electrophoretic deposition, painting, dip coating) were essential for obtaining uniform, protective coatings on integral vane rings and integrally bladed rotors. Subsequently, coating development for silicon nitride focused on non-line of sight coating methods. The most promising processing routes were found to be slurry coatings and CVD.

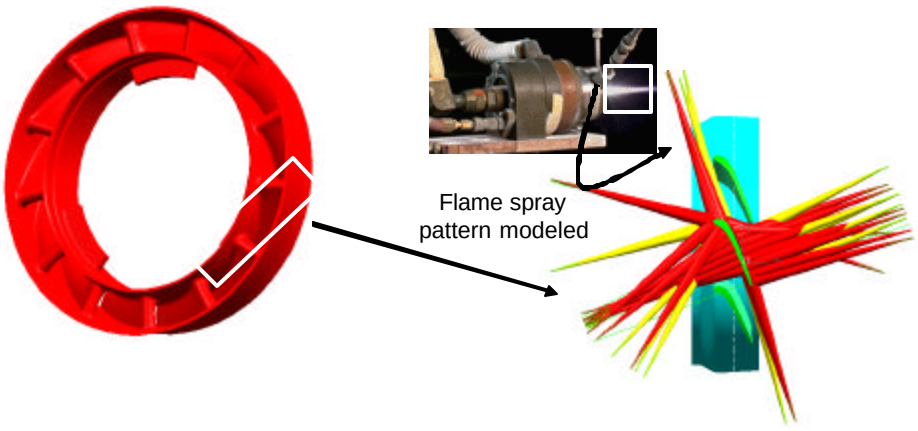

Figure 9: Study of the feasibility of thermal spraying an integral vane ring.

Bond Coat Development

Early work on the development of EBC for silicon nitride (Si_3N_4) was done under the NASA EPM, DOE CSGT and DOE/ONR funded EBC for Silicon Nitride programs. The EBC developed for silicon carbide (SiC) has been demonstrated to be ineffective for Si_3N_4 as it caused a debit in room temperature (RT) strength of the base material by over 50%. Figure 10 shows the reduction in strength when the 3-layer state-of-the-art EBC_{SiC} is applied to silicon nitride (AS800). A similar strength debit was also seen on other grades of silicon nitride and at elevated temperature the debit in strength was ~15%. The primary mechanism causing the reduction in the strength of silicon nitride has been identified to be the thermal mismatch between the coating and silicon nitride. It was also found that the application of the silicon bond coat alone to the substrate (with or without a top layer) results in about 50% debit in room temperature strength of the substrate indicating that the silicon is the "weak-link" in the coating system. The coatings are typically very well bonded to the substrate and the CTE mismatch cracks are expected to interact with the pre-existing cracks in the ceramic resulting in a significant reduction in fracture strength of the ceramic.

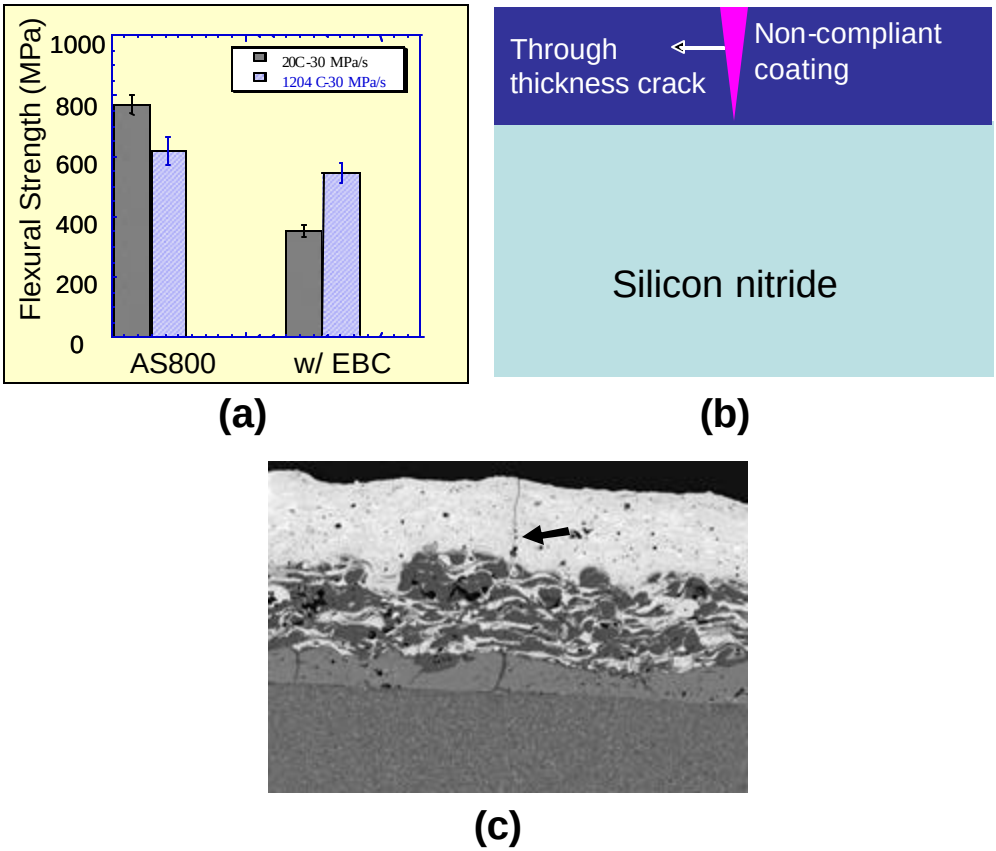

Figure 10: (a) Effect of BSAS-based EBC coating on strength of Si_3N_4. (b) Schematic mechanism of strength reduction. (c) Microstructure of BSAS EBC on Si_3N_4 that shows the flaws in the coating.

Under this program, further efforts were made to understand the mechanism for the strength debit of the substrate using numerical modeling. When a thin layer of silicon is

deposited on a silicon nitride substrate and the system is cooled from a stress-free temperature of 1000°C (1832°F), the in-plane tensile residual stress in silicon given by, [$\sigma = E\Delta\alpha\Delta T/(1-\upsilon)$]; where E is the modulus of silicon, $\Delta\alpha$ is the difference in CTE of silicon and silicon nitride, ΔT is the temperature difference and υ is the Poisson's ratio, is of the order of 26 ksi (=179 MPa) which far exceeds the published values of tensile strength of silicon. The magnitude of tensile stress in silicon is fairly independent of thickness of silicon layer, and thickness and moduli of intermediate and top layers, as long as thickness of coating layers is at least an order of magnitude lower than the substrate thickness (which is typically the case in most applications), as shown in Figure 15 below.

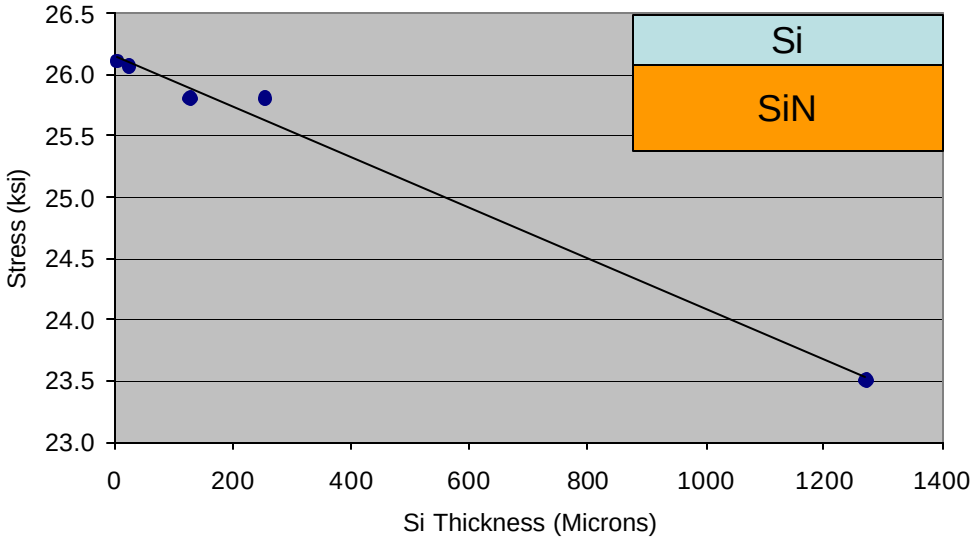

Figure 11: Calculation of residual stress in Si layer on monolithic Si_3N_4. The stress in the coating is fairly independent of the coating thickness.

A variety of coating architectures were considered with an objective to drive down the residual stress in the silicon layer. Some of the architectures are shown in Figure 12 below. The thermophysical properties of the layers were varied and it was found that if the CTE of the materials was varied within 4 ppm/C of Si_3N_4, the residual stress in the silicon layer did not decrease to levels much lower than 23-25 ksi.

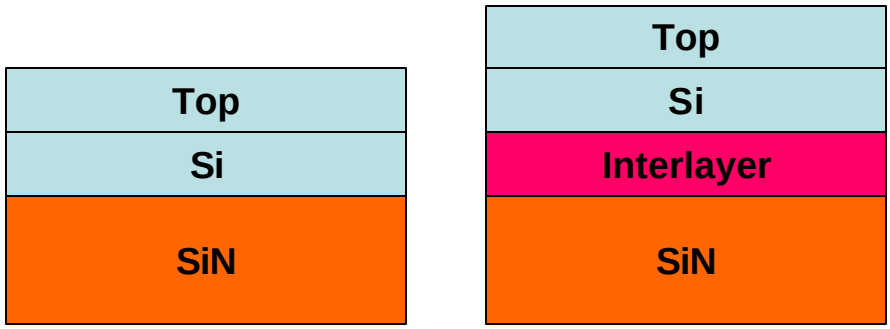

Figure 12: Various architectures considered to drive down residual stress in the Si-layer of the coating.

In addition to the stress analyses, micromechanical fracture modeling was also conducted to explain the effects of residual stress in the Si layer on flaw creation, propagation and interaction with pre-existing flaws in silicon nitride. It was determined that using a low modulus interlayer between Si_3N_4 and silicon helps in isolating the flaws in the coating from the pre existing flaws in Si_3N_4.

Subsequent processing refinement resulted in the down-selection of a low modulus oxide-based interlayer between Si_3N_4 and Si. The coating was found to help retain the strength of Si_3N_4 as is shown in Figure 13 below. The figure also shows a typical microstructure of the bond coat system. A well adhered gas tight top layer will be necessary to provide the steam protection required in the gas turbine environment.

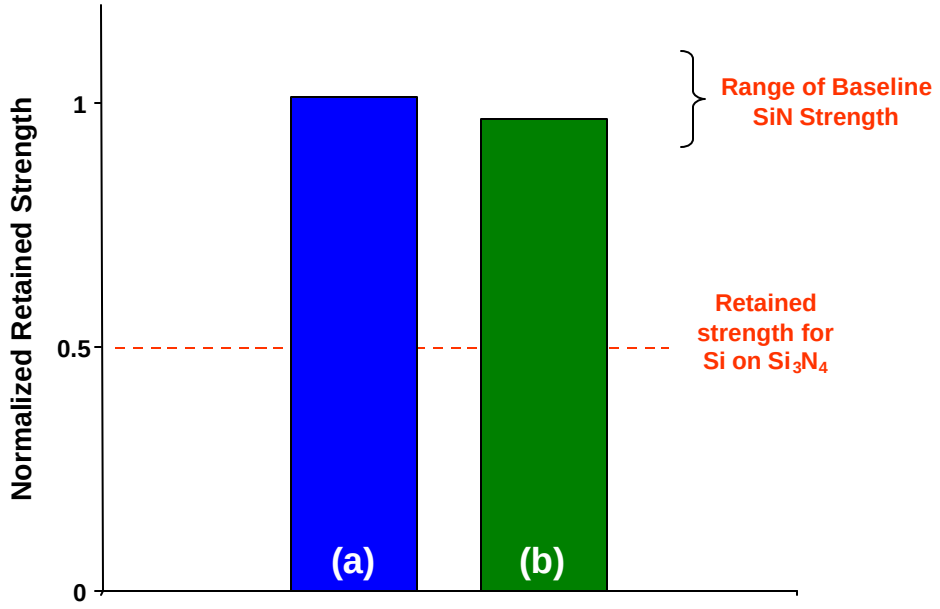

Retained strength with (a) 35 mm and (b) 70mm thick silicon layer on oxide interlayer

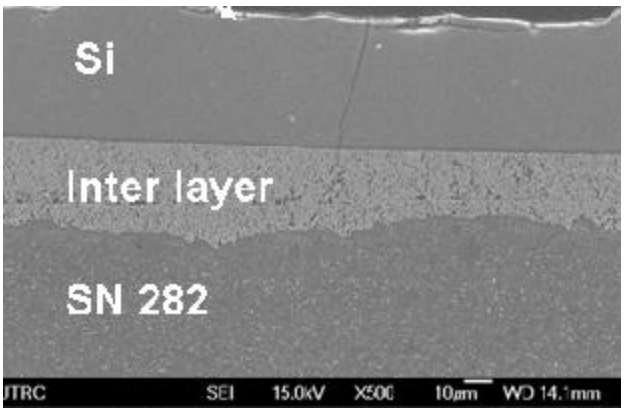

(b)

Figure 13: Retained strength of silicon nitride using oxide-based interlayer between silicon nitride and silicon bond coat.

Top Layer Development

The purpose of the top layer(s) deposited on the bond coat system described above is to provide environmental protection against high pressure, high velocity steam at high temperatures (2200-2400°F). While it is acknowledged that the ability to provide environmental protection is highly dependent on the microstructure of the coating (density and adherence), which in turn depends upon the processing route used, the intrinsic material stability in a steam rich combustion environment is critical. Several simple and complex oxides were evaluated in the UTRC steam rig (90% steam, 1 atm; 5 cm/s flow velocity). The processing of environmental barrier top layers by non-line-of-sight methods is being continued under the DOE Advanced Microturbine Contract.

2. Design and Testing of Ceramic Components

Ceramic Matrix Composites (CMCs) are considered an enabling turbine engine material because of their high thermal-mechanical performance and low density compared to metal alloy and intermetallic materials. Furthermore, CMCs have demonstrated improvements in apparent toughness and failure strain compared to monolithic ceramic materials[7]. The introduction of CMC combustor liners in industrial gas turbines (IGTs) with premixed combustors has resulted in reduced emissions and higher cycle efficiency[8]. More recently, CMC turbine vanes have also been designed and rig tested in representative environments[9,10].

Ceramic matrix composites (CMCs) protected with environmental barrier coating offer an approximately 225-325°C (400-600°F) temperature capability increase over thermal barrier coated Hastelloy X alloy. When applied to gas turbine combustor liners, such a superior temperature capability translates to less cooling air requirement, smaller pressure losses, lower NOx and CO emissions, and better flame stability. The technical objectives of the task are two fold: 1) prove the applicability of CMC materials to gas turbine combustor liners, and; 2) demonstrate the benefits of CMC combustors liners.

Pratt & Whitney's FT8, an aero-engine derived industrial gas turbine (IGT), has a power output of 27 MW and an efficiency of 37% with natural gas in electrical power generation applications. This engine is currently in use for power generation, natural gas pumping, and marine applications worldwide. CMC combustor liners were designed and the technology was demonstrated in a FT8 sector-rig at UTRC.

2.1 Mechanical Design

One of the key challenges in designing with the ceramic components is developing an attachment methodology that minimizes the high thermal stresses that are generated due to thermal expansion mismatch between the low CTE ceramics and high CTE metallic components. In addition to the CTE mismatch induced thermal stresses, the CMC combustor is also subject to high mechanical loads due to differences in the internal and external pressures on the liner.

In the conceptual design phase, special attention was paid to attaching the CMC combustor liner to a metal support so that thermal stress due to differential thermal growth between the metal support and the CMC combustor liner is minimized. Several attachment concepts were generated and a final down-select was made based on the ease of manufacturing, attachment stress, leakage control, effect on combustion process, emissions benefit, and production cost. In order to have a one-on-one comparison of emissions between the metal and CMC liner, the flow through the combustor was kept the same as the current FT8 engine. To keep the same flow rate (and pressure drop) as the metal liner, the film-cooling air was redirected to enlarged dilution holes in the CMC combustor liner.

The preliminary and detailed design efforts focused on the details of the front attachment area and CMC liner exit area. Various means to accommodate thermal growth differential were considered and analyzed in detail. Thermal, stress and dynamic analyses were performed and the results indicated that temperature, stress and dynamic frequencies are all within the design allowables. Figure 14 shows the CMC temperature distribution and Figure 15 shows the in-plane axial stresses. For reference, the average tensile strength of melt infiltrated (MI) SiC/SiC CMC with Sylramic^{TM} fibers is 50-70 ksi with a proportional limit of 20-25 ksi.

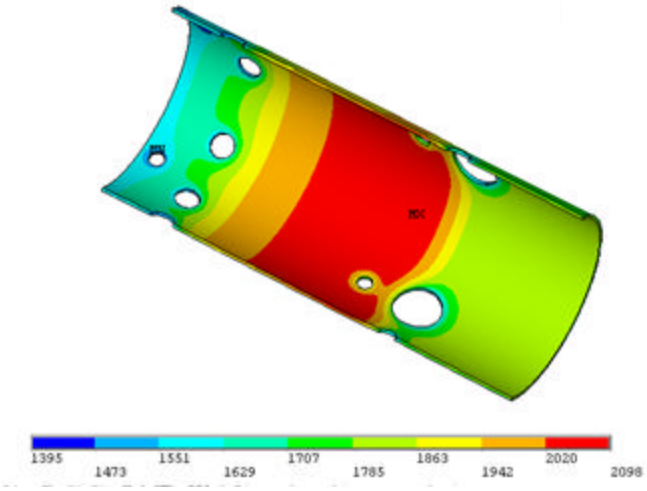

Figure 14: Temperature distribution (in F) inside the CMC combustor liner

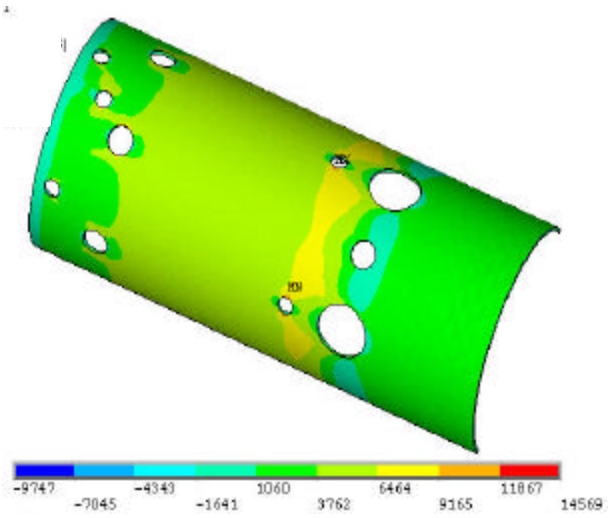

Figure 15: In-plane axial stress (in psi) in CMC combustor liner

2.2 Emissions Modeling

The current bill-of-material metallic combustor liner is actively cooled with a film via a series of louvers along the length of the liner. The diffusion combustor is injected with water in order to control the NOx emissions. The mechanism for the reduction of NOx emissions with added water is well established. Primarily, NOx is reduced by lowering the peak flame temperature at stoichiometric conditions. In addition, there are secondary chemical kinetic mechanisms that decrease NOx levels[11]. The addition of water can also lead to lower CO emissions by shifting the equilibrium $H_2O + CO \rightarrow CO_2 + H_2$ towards CO_2. Normally, this effect cannot be observed as this process is limited by slow kinetics. The film cooling in the conventional metal liner exacerbates the quenching and produces high amounts of CO emissions with increase in water injection.

Stirred reactor network modeling, where a series/parallel set of individual perfectly stirred reactors (PSRs) is coupled to simulate a combustor, was used to predict the effects of film cooling on CO emissions. The liner was divided into two parts radially, the center core PSRs (No. 1 to No. 28) and the boundary layer PSRs (No. 29 to No. 56). Axially, the liner is divided into five large zones, each of which is divided into a number of small volumes in order to capture the transition of fuel rich to fuel lean regions and the detailed location of dilution and/or cooling air. Figure 16 shows the center core and boundary layer PSR network that was used for modeling the emissions. Mass flows, local equivalence ratios, and volumes are selected by the user and the combustion chemistry is treated by a detailed chemical kinetics model. A network was initially developed based upon extensive engine data with the conventional FT8 metal liner and was extended to treat the CMC liner. In the case of metal liner, the cooling air is injected into the boundary layer PSRs. For each axial stage, interchange of the flow between the center core and the boundary layer was assumed to be 6% of the core flow and from the boundary layer to the center core was 0.4% of the boundary layer flow. The interchange does not apply to the quench zone since it is assumed that there is not enough time for mass exchange to occur.

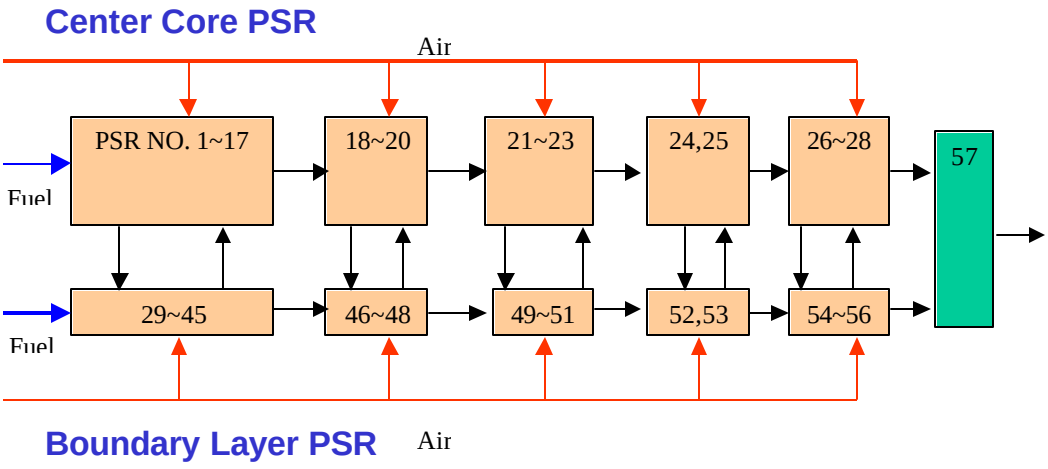

Figure 16: Center core and boundary layer PSR network

The network was tuned to reproduce the NOx emissions for the metal liner at no water injection conditions. This involved careful simulation to capture the transition between the fuel rich gases in the front end to the overall lean conditions downstream. At baseload with no water injection, the CO levels are near equilibrium and so the results are fairly insensitive to the reactor structure. The CO curves were fitted by varying the boundary layer reactors and mass interchange with the core.

Calculations were performed for both CMC and metal liners with and without water injection. Figure 17 shows the trade-off of NOx and CO for the metal liner with increasing water injection. NOx (sum of NO and NO_2) and CO emissions are represented by a standard concentration (ppmvd @15% O_2), which is the concentration of NOx and CO in the products at a condition where O_2 is 15% without water.

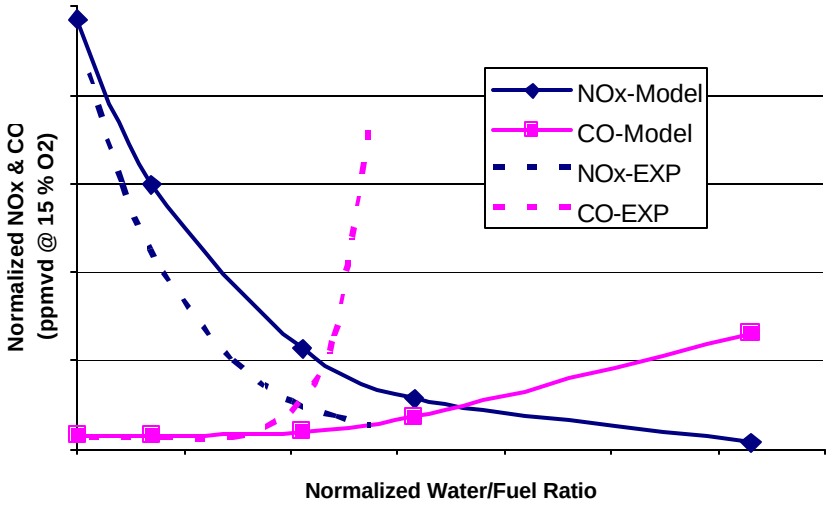

Figure 17: NOx and CO emissions versus water to fuel ratio

Comparison of simulation and experimental data indicates that the computed NOx decreases more slowly as water/fuel ratio increases. In addition, CO increases more gradually in the simulation than in the experiment with increase in water injection. A probable explanation for this discrepancy is that the latent heat of water vaporization is not accounted in the computation. In the current PSR network code, water is injected with fuel as a gaseous species, whereas in the rig and engine tests, water is injected as liquid. The heat of vaporization of water would further reduce gas temperature and more natural gas would be required to maintain the gas temperature. Nevertheless, peak temperatures under stoichiometric conditions would be reduced, thus lowering NOx production and emissions. Therefore, the model would underestimate the effect of the added water on NOx emissions (as depicted in Fig. 17). There is also a difference between the experimental CO emissions and those predicted by the PSR modeling. CO levels should be more pronounced with lower stoichiometric flame temperatures from a

kinetics viewpoint. Thus CO levels should increase more rapidly with water addition if the heat of vaporization of water were included. A contributing explanation for this discrepancy between the experimental and modeled emissions may be related to the fact that the model cannot treat dissimilar distributions of natural gas and fuel at the front end. The water is equally distributed with the fuel in the present study. With increased water/fuel ratios, a greater fraction of the water may be injected to the walls that further quench the CO oxidation. Such effects were not captured in the present model.

With the network of PSRs calibrated for the metal liner combustor (at least with recognized uncertainties/errors), the network was applied to the CMC liner. As described previously, in the case of CMC liner, the film cooling air from the wall was simply reallocated to the main quench/dilution holes to ensure that the boundary layer did not become overly lean and quench the CO, as the metal combustor liner. Figures 18 and 19 show the CO concentrations in the center core and boundary layer PSRs for CMC and metal liners. The figures show that the center core PSRs have similar levels of CO but the CO mole fractions in the boundary layer PSRs are much higher for the metal liner than for the CMC liner. This is because a large amount of cooling air is injected into the boundary layer PSRs for the metal liner. Hence, the temperature at the boundary layer is much lower and CO oxidation is quenched, leading to higher CO levels for the metal liner. Based on these results, a 2-3x improvement in CO emissions at the same NOx levels is predicted for CMC versus metallic liner.

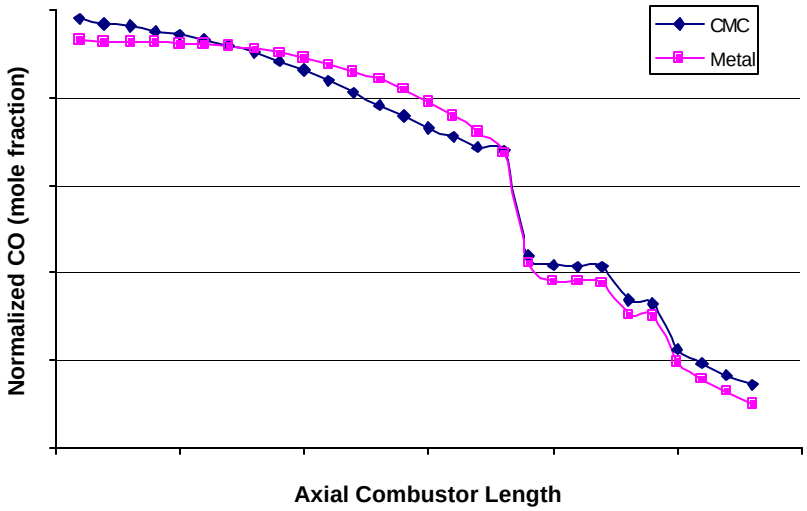

Figure 18: CO emissions at the center core PSRs for metal and CMC liners

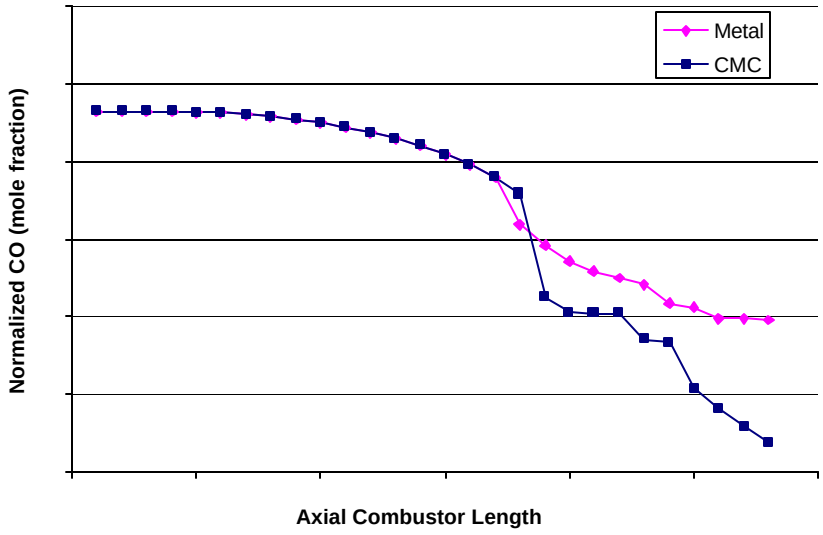

Figure 19: CO emissions at the boundary layer PSRs for metal and CMC liners

2.3 Fabrication

Two silicon carbide fiber reinforced silicon carbide matrix (SiC/SiC) CMC combustor liners were fabricated by Goodrich Corporation via the standard slurry cast / melt infiltration (MI) process (see Table 3). The first liner was reinforced with Sylramic^{TM} fiber produced by Dow Corning Corp. and was fabricated under the contract. The preform was created by handed lay-up of twelve plies of 5 harness satin weave fabric (5HS) in a 0/90 orientation (Figure 20). The ply joints were staggered and created using the NASA fringe joints. Under the NASA funded Enabling Propulsion Materials (EPM) program the fringe joints produced superior performance compared to the standard butt joint (Figure 21). The second liner was fabricated under Goodrich's internal funding. It was reinforced with Tyranno ZMI fiber in a tri-axial braided architecture.

Table 3: Lay-up and physical characteristics of the two MI SiC/SiC liners fabricated

Material	Sylramic	Tyranno ZMI
Fiber	Sylramic	Tyranno ZMI
Cloth Layup	2D 5HS	2D Braid
Axial Fibers	50%	11%
Hoop Fibers	50%	None
Bias Fibers	None	89%
Braid Angle	N/A	75 Deg
Number of Plys	12	8
Joints	Fringe Joints	None
Fiber Volume %	35-36	35-37
Porosity	7%	3%

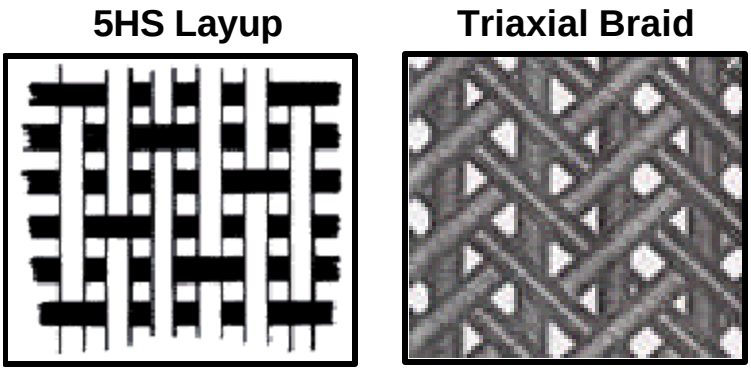

Figure 20: CMC fabric: 5-harness satin fabric (left) and tri-axial braid (right)

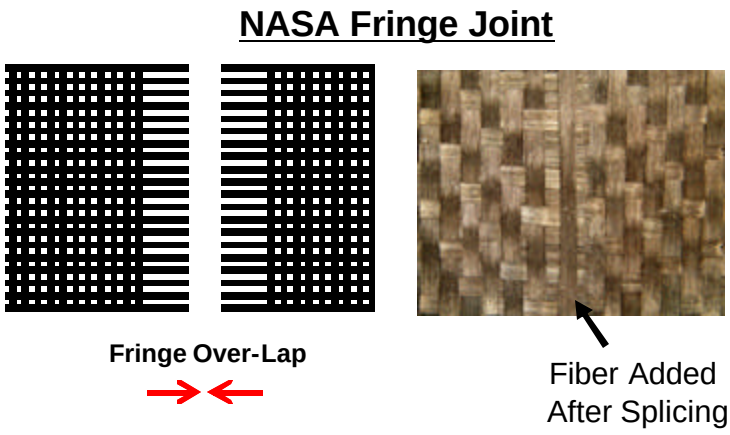

Figure 21: NASA fringe joint used on 0/90 Sylramic fiber liner

After MI SiC/SiC processing attachment and dilution holes were laser machined in both liners as shown in Figure 22. After machining, the liners were EBC-coated on the inner diameter with SAS-based coating.

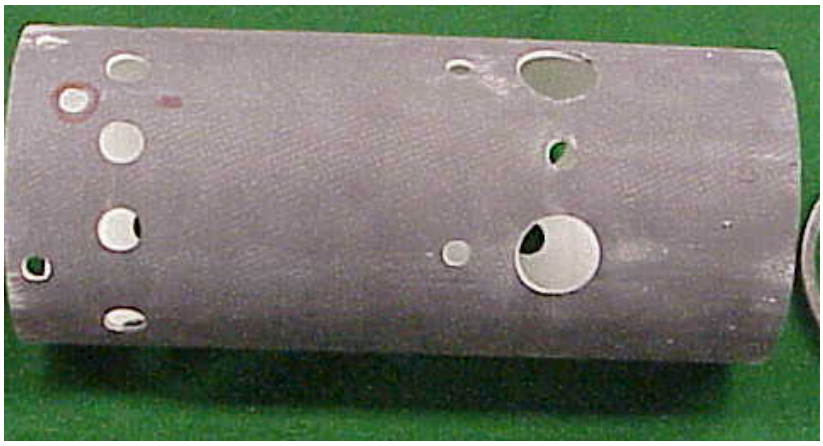

Figure 22: EBC-coated CMC combustor liner for sector-rig test

2.4 Characterization of CMC Liners

The MI SiC/SiC liners were characterized by destructive and non-destructuctive techniques to evaluate their quality for rig testing. Destructive techniques included burst testing and microstructural examinations whereas the non-destructive techniques used were computer tomography (CT) and ultrasonic scan.

The liners were made with extra length so that several rings could be laser machined off the ends for burst testing. The room temperature burst testing was performed by Southern Research Institute using an internal bladder to provide internal loading. The burst test strength and elastic modulus data is presented in Table 4 and flat panel tensile data is provide for comparison. The burst test loaded the composite rings in the hoop direction which is the bias direction for the braided composite. The proportional limit of the burst test rings were lower but close to the values for flat panels. The high hoop (bias) strength and low axial strength in the braided liner is due to the liner having 89% of the fiber in the bias direction and 11% in the axial direction.

Table 4: Mechanical properties of the SiC/SiC CMC liners: Ring burst test and flat panel data

	Burst Test (ring)			0 / Bias Tensile (panel) *			90 / Axial Tensile (panel) *		
Type of Liner	Max. Stress (ksi)	Prop. Limit (ksi)	Modulus (Msi)	Max. Stress (ksi)	Prop. Limit (ksi)	Modulus (Msi)	Max. Stress (ksi)	Prop. Limit (ksi)	Modulus (Msi)
0/90 Sylramic Liner	24	20	33	49	25	35	49	25	35
Braided ZMI Liner	28	20	30	49	20	33	8	6	17

* Panel data measured by Goodrich Corp.

CT scan was performed using an industrial CT scanner with 420 KeV X-ray source with a linear detector array. The liner was scanned with 0.5mm vertical spacing by 0.3mm aperture. The raw measurement data was reconstructed into several images with 1024x1024 pixels each, from which a 3-dimensional model was created. The 3D model was then aligned and compared to the CAD model to determine dimensional accuracy and porosity distribution, as shown in Figure 23 below. The variation in porosity levels is also shown in ultrasonic scans (Figure 24).

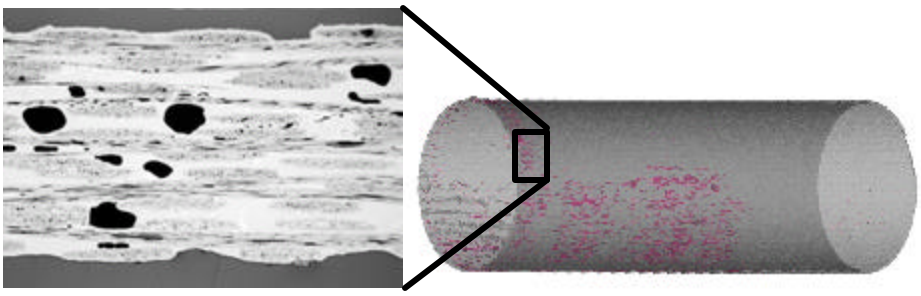

(a) 0/90 Sylramic liner, ~7% porosity

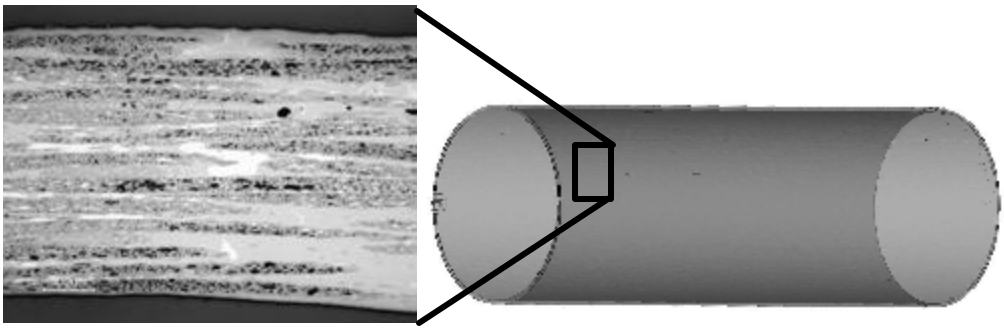

(b) Braided ZMI liner, < 3% porosity

Figure 23: Residual porosity in the CMC combustor liner and 3-D image created from CT scan data

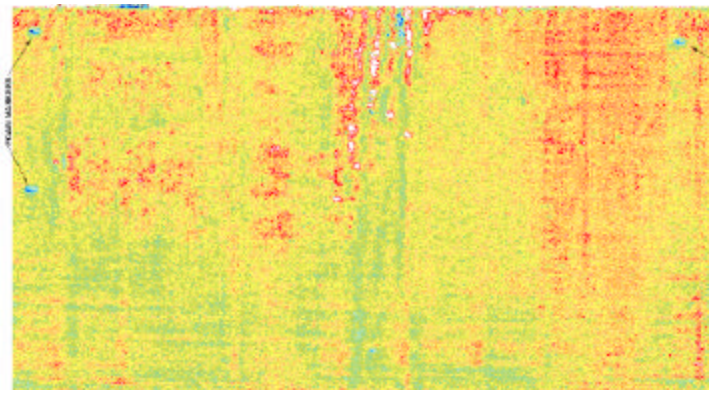

(a) 0/90 Sylramic liner, higher variation in color correlates to 7% porosity

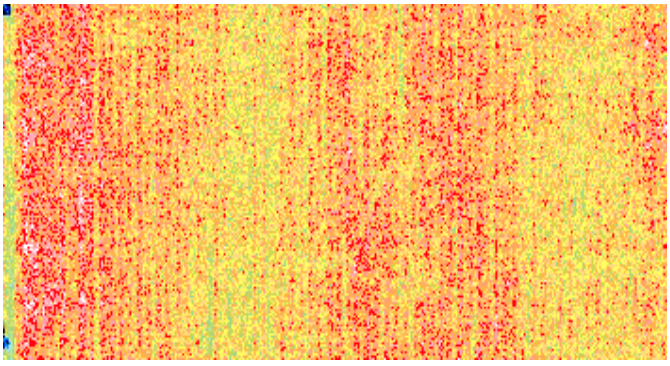

(b) Braided ZMI liner, lower variation in color correlates to < 3% porosity

Figure 24: Ultrasonic scans on MI SiC/SiC liners

As discussed previously, recent work showed that SAS based coatings are projected to have a longer life than BSAS based coatings due to better steam stability and higher SAS/Mullite eutectic temperature compared to BSAS/Mullite. SAS based EBCs have been tested in Solar Centaur 50S combustor liners for 8,348 hours[12]. The FT8 CMC combustor liners were coated with silicon bond coat, mullite intermediate coat and SAS top coat. Figure 25 shows the microstructure of the EBC coating on the CMC liner.

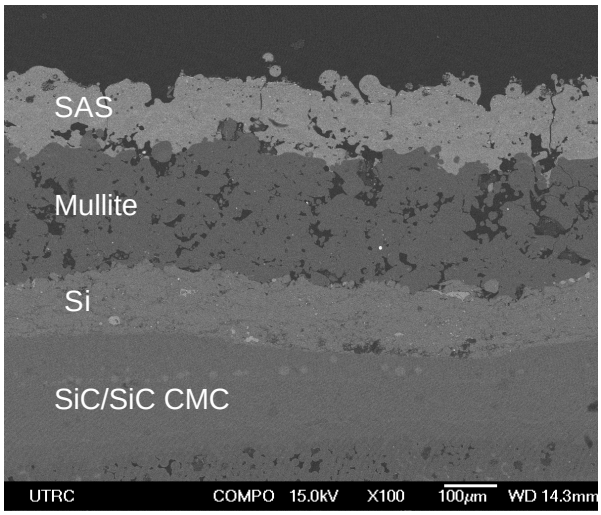

Figure 25: EBC coating on CMC combustor liner

2.5 Sector-rig Test

The CMC combustor liner was tested in a FT8 sector rig at UTRC that simulates the engine conditions very well. The rig utilizes a single can of the nine cans in a FT8 engine, along with a 40-degree arc slice of the combustor to high pressure turbine transition duct. The rig is fed compressed air from a mechanical compressor and is then heated by a natural gas fired vitiated heater to simulate T3 air coming from a compressor in an actual turbine. The rig is capable of testing to 100 percent of engine temperature, and 90% of maximum engine pressure conditions. Figure 26 shows a schematic of the FT8 sector-rig with metal combustor liner. The vanes were instrumented with thermocouples to detect any sudden mechanical failure, and pressure taps to measure the pressure drop across the baffle/vent cooling system. The combustor transition duct periphery was also instrumented for pressure and temperature measurements. Initial shakedown testing was performed using warm T3 air. The sector was then lit off and fuel and airflows were set to emulate FT8 operation at 50 to 85% of full power condition.

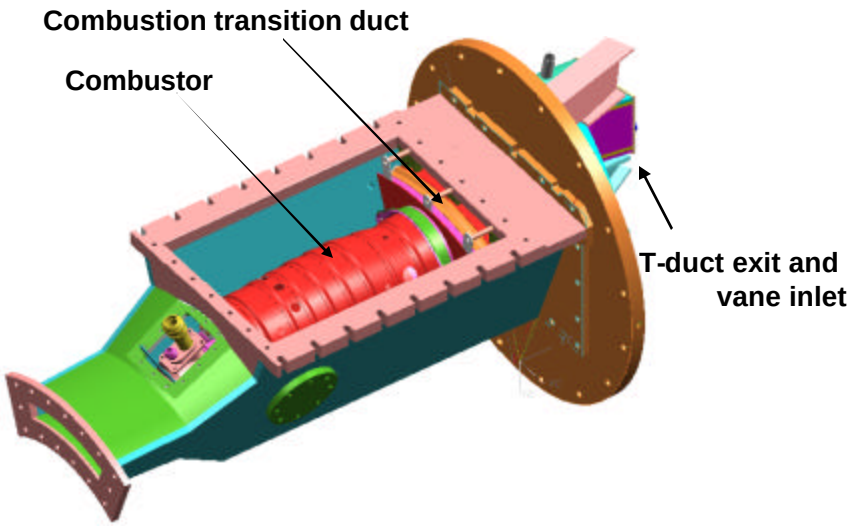

Figure 26: Schematic of FT8 sector rig

The emissions profile (NOx and CO) was measured during the test under various conditions including part load (50 to 85% power), with and without water injection, and with natural gas and liquid fuels. A baseline metal combustor liner was tested at various conditions to ensure rig operability. The data from the metal combustor liner was found to be consistent with prior rig and FT8 engine test data. The test points were repeated for the CMC combustor liner and NOx and CO emissions were measured via fully-instrumented vanes downstream of the transition duct.

Figure 27 below shows the normalized CO and NOx emissions at 15% oxygen levels. Under dry conditions, the NOx levels are fairly high and as the water is injected, the NOx decreases. At certain water to fuel ratio (nominally 0.8 to 1.2), the CO increases asymptotically to fairly high levels. The figure shows NOx/CO emission tradeoff from current bill of material film-cooled metallic combustor liner, a partially cooled CMC liner and an uncooled CMC liner. As shown in the plot, the CMC liners demonstrated significant improvements (2-6x reduction) in the CO emissions at the same NOx levels at various load conditions depending upon the amount of cooling air in the liners. The mechanical design and CMC to metal attachment methodology were also validated by the sector rig test. The CMC liners survived several unexpected trip shutdowns from 50 to 75% load levels.

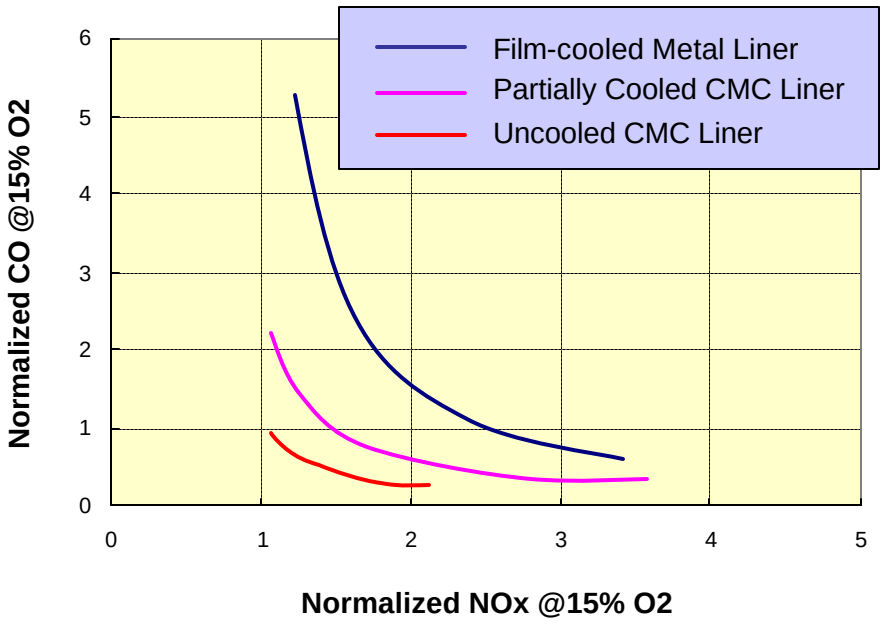

Figure 27: CO and NOx emissions profile from metal and CMC combustor liners

2.6 Post-test Analysis of the Combustor Liners

After the successful completion of the FT8 sector rig test, the EBC coated CMC liners were characterized to evaluate the coating and the SiC/SiC CMC substrate. Visual inspection of the EBC coated Sylramic combustor liner showed a yellow discoloration of the coating surface (Figure 28). The staining of the EBC was determined as due to the presence of iron, calcium and magnesium deposits. In addition, the coated surface appeared glazed after the uncooled CMC liner test, likely due to the increased temperature of the EBC/CMC and local glass formation. The combustor liners were cross-sectioned for post-test metallographic examination. The glassy material was analyzed for composition and Ca and Mg were found. The origin of these alkaline materials was traced to the city water used during the test to control NOx emissions. Lab scale furnace experiments were conducted to validate that the glass formation was due to the city water. There was no glass formation observed when EBC-coated CMC coupons were immersed in deionized water at 2200°F (and above) whereas identical tests carried out with city water showed the formation of glass on the surface. The specifications for water-injected diffusion combustors in industrial gas turbine engines (IGT) typically require use of deionized water and therefore such effects (local glass formation or glazing) are not expected in EBC coated CMC combustors liners.

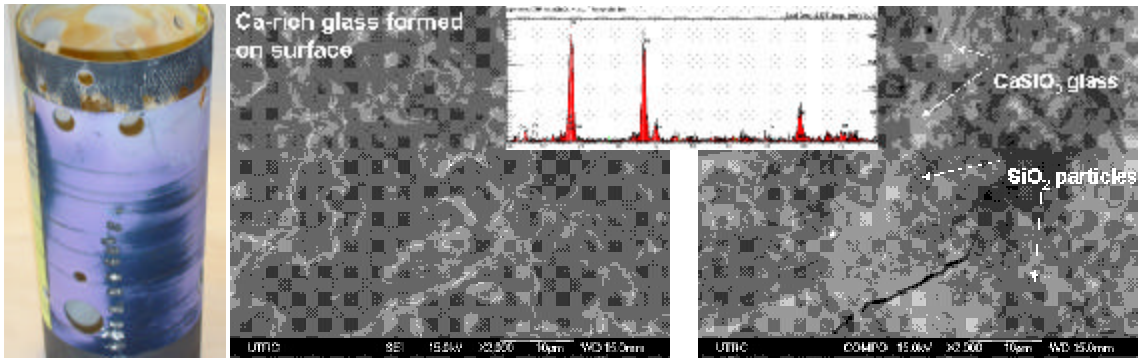

Figure 28: Post test analysis of the CMC liner showing the Ca and Mg rich glaze on the surface

The other finding from metallographic examination at the aft-end of the Sylramic liner was melting of Si in the bond coat and CMC as shown in Figure 29 below. The melting of the Si was only found in the aft end of the liner indicating that the temperature in this section reached over 2500°F. The high temperatures were attributed to a minor design issue that resulted in the lack of backside cooling on the liner aft end.

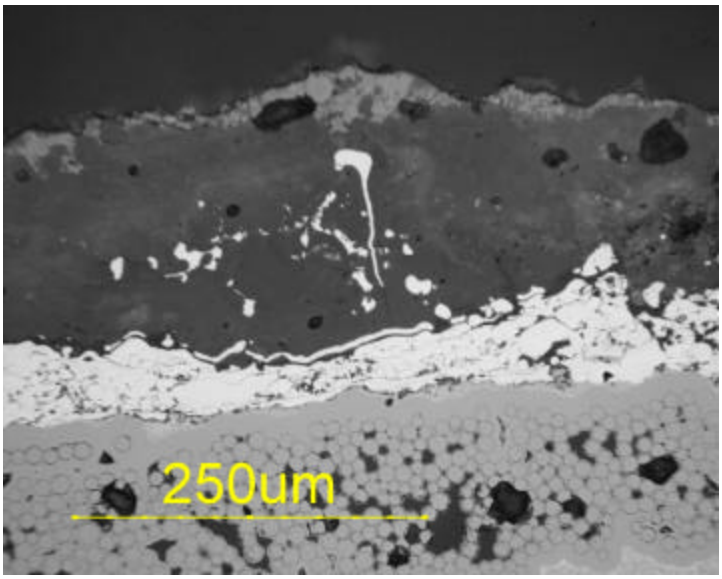

Figure 29: Melting of Si observed in the aft end of the combustor liner.

3. Development of Silicon based Substrate Material

The objective of this task was to examine whether a silicon carbide based material can be developed for ceramic turbine components that would be compatible with the EBC developed for SiC/SiC composites. Elongated grains (platelets) are desired to increase the fracture toughness instead of utilizing fiber reinforcements. Addition of a refractory, but low elastic modulus second phase was used to reduce the overall material's elastic modulus to reduce thermal and mechanical stresses generated during the operation of the gas turbine engine.

A limited number of initial hot pressing trials were performed using beta silicon carbide and a glass-ceramic as the low modulus second phase to demonstrate the proof of concept. The resultant material met elastic modulus goals at approximately 38 Msi (260 GPa), however strength levels were limited to ~60 ksi. During cyclic oxidation to 1300ºC, the secondary glass-ceramic phase appeared to exude out and form bubbles. The majority of efforts were then focused on developing a porous sintered body with a secondary phase infiltration as the final processing step. The objective was to minimize densification and shrinkage of the sintered body, while forming plate-like and elongated grains. Two approaches were considered; the first one focused on the use of oxide based sintering additives while the other focused on the use of metallic sintering aides. Several trials were made using two different oxide sintering aid mixtures and both routes resulted in elongated grain microstructures. Careful measurements of test samples before and after sintering indicate that shrinkage values were in the range of 0.1 to 0.2%. Difficulties were encountered during infiltration of the second phase. It is conjectured that the oxide sintering additives may prevent wetting of the second phase. Subsequently, a separate chemical treatment to change the post-sintered material's surface chemistry was conducted, and second phase infiltration was accomplished that resulted in strengths between 60 and 100 ksi.

Following completion of the work described above, efforts in this area are continuing under a U.S. Army contract (W31P4Q-05-D-R002). A dry pressing binder has been developed, and integral vane rings are being prototyped via iso-press and green machining approach.

4. Summary

The objective of this contract was to develop technologies critical for ceramic hot section components for gas turbine engines. Significant technical progress has been made towards maturation of the EBC and CMC technologies for incorporation into gas turbine engine hot-section. Promising EBC candidates for longer life and/or higher temperature applications relative to current state of the art BSAS-based EBCs have been identified. These next generation coating systems have been scaled-up from coupons to components and are currently being field tested in Solar Centaur 50S engine. CMC combustor liners were designed, fabricated and tested in a FT8 sector rig to demonstrate the benefits of a high temperature material system. Pretest predictions made through the use of perfectly stirred reactor models showed a 2-3x benefit in CO emissions for CMC versus metallic liners. The sector-rig test validated the pretest predictions with >2x benefit in CO at the same NOx levels at various load conditions. The CMC liners also survived several trip shut downs thereby validating the CMC design methodology. The next steps are to develop an understanding of the life limiting mechanisms in EBC and CMC materials and conduct system-level technology demonstration via a full scale gas generator or an engine test.

References

[1] "Oxidation of Silicon Carbide Refractory Materials", A.C. Lea, J. Soc. Glass Technology, 33 [150] 27-50T (1949); Ceram. Abstr., 1951, Novemebr, p. 198f.

[2] "Paralinear Oxidation of CVD SiC in Water Vapor", E.J. Opila and R.E. Hann Jr, J. Am. Ceram. Soc., 80 (1), p. 197-205 (1997).

[3] "Mass Spectrometric Identification of Si-O-OH(g) Species from the Reaction of Silica with Water Vapor at Atmospheric Pressure", E.J. Opila, D.S. Fox, and N.S. Jacobson, J. Am. Ceram. Soc., 80 (4), p. 1009-12 (1997).

[4] "SiC Recession Caused by SiO_2 Scale Volatility under Combustion Conditions: II, Thermodynamcis and Gaseous-Diffusion Model", E.J. Opila, J.L. Smialek, R.C. Robinson, D.S. Fox, and N.S. Jacobson, J. Am. Ceram. Soc., 82 (7), p. 1826-34 (1999).

[5] "SiC Recession Caused by SiO_2 Scale Volatility under Combustion Conditions: I, Experimental Results and Empirical Model", R.C. Robinson and J.L. Smialek, J. Am. Ceram. Soc., 82 (7), p. 1817-25 (1999).

[6] "EBC Protection of SiC/SiC Composites in the Gas Turbine Combustion Environment", H.E. Eaton, G.D. Linsey, K.L. More, J.B. Kimmel, J.R. Price, and N. Miriyala, ASME 2000-GT-631, Munich 2000.

[7] "Ceramic Gas Turbine Design and Test Experience", M. van Roode, M.K. Ferber, and D. Richerson, Progress in Ceramic Gas Turbine Development, Vol. 1, Eds, ASME Press, New York, 2002.

[8] "The Evaluation of CFCC Liners After Field Testing in a Gas Turbine – IV", J. Kimmel, J. Price, K. More, P. Tortorelli, E. Sun, and G. Linsey, Proceedings of Turbo Expo 2003, Power for Land, Sea, and Air, June 16-19, Atlanta, Georgia, ASME Paper GT2003-38920.

[9] "Ceramic Matrix Composite Vane Subelement Testing in a Gas Turbine Environment", M. Verrilli, A. Calamino, R.C. Robinson, and D.J. Thomas, Proceedings of ASME Turbo Expo 2004, Power for Land, Sea, and Air, June 14-17, 2004, Vienna, ASME Paper GT2004-53970.

[10] "Ceramic Matrix Composite Vanes for Gas Turbine Engines", V. Vedula, J. Shi, D. Jarmon, S. Ochs, L. Oni, T. Lawton, K. Green, L. Prill, J. Schaff, and G. Linsey, Proceedings of ASME Turbo Expo 2005, Power for Land, Sea, and Air, June 6-9, 2005, Reno, Nevada, ASME Paper GT2005-68229.

[11] "An Experimental and Modeling Study of Humid Air Premixed Flames", A. Bhargava, M. Colket, W. Sowa, K. Castleton, and D. Maloney, ASME Journal of Engineering for Gas Turbines and Power, Vol. 122 (3), 405-411, 2000.

[12] "The Evaluation of CFCC Liners After Field Testing in a Gas Turbine – V", J. Kimmel, J. Price, K. More, P. Tortorelli, T. Bhatia, and G. Linsey, Proceedings of Turbo Expo 2005, Power for Land, Sea, and Air, June 6-9, Reno, Nevada, ASME Paper GT2005-68961.

Acknowledgements

This work and the efforts leading to it would not have been possible without the guidance and support of the Office of Naval Research (ONR) [Drs Steven Fishman and David Shifler] and the Department of Energy (DoE) Distributed Energy (Office of Electricity) [Deborah Haught and Don Geiling]. The cost sharing provided by the United Technologies Corporation is gratefully acknowledged. In addition, many other UTRC and Pratt & Whitney personnel helped make this project a success including the following:

UTRC
Bob Barth
Tania Bhatia
David Bombara
Bob Brown
Chuck Burila
Shaoluo Butler
Louis Chiappetta
Owen Donohue
Graham Fulton III
Steve Gore
Mark Hermann
John Holowczak
Glenn Janowsky
David Jarmon
Scott Kearney
Jason Lawrence
Thomas Lawton
Bruce Laube
Gary Linsey
Fred Lussier
Lola Oni
Wayde Schmidt
Jun Shi
John Smeggil
G.V. Srinivasan
Xia Tang
Bill Tredway
Jodi Vecchiarelli
Mike Weber
Jim Wilkinson
Roy Wong
Phil Vecchiarelli
Albert Veninger

Pratt & Whitney
Barry Schlein
Richard Tuthill

Final Contract Report
Office of Naval Research N00014-06-C-0585

"Enabling Technologies for Ceramic Hot Section Components"

Volume 2

Tania Bhatia
Program Manager

United Technologies Research Center
M/S 129-88
411 Silver Lane
East Hartford, Connecticut 60108

January 30, 2009

TABLE OF CONTENTS

LIST OF FIGURES

LIST OF TABLES

1.0 Durability Evaluation of Uncoated and EBC-coated CMC Materials

1.2 Background

In 1949 and 1951, A.C. Lea[1] studied and reported on the rate of oxidation of silicon carbide and noted that steam caused the oxidation rate to be accelerated compared to the rate in dry oxygen. The volatilization of silica in an air-steam atmosphere was presented as a possible mechanism to explain the observation. Almost 50 years later, Opila and Hann[2], Opila, Fox, and Jacobson[3], and Opila, Smialek, Robinson, Fox, and Jacobson[4] studied in detail and presented a model explaining the accelerated oxidation of silicon carbide due to high temperature exposure to steam. Their work showed that, on exposure to steam, oxidation of silicon carbide occurs by a paralinear rate process involving oxidation of silicon carbide by H_2O to form silica and then volatilization of the silica by reaction with H_2O to form Si-O-H(g) species (see equations 1 & 2). For overall paralinear behavior, the silica layer that forms on the substrate due to oxidation occurs by a parabolic rate process while the volatilization of the silica occurs by a linear rate process. Over long times, the growth rate process of silica formation is balanced by the volatilization process at which time further oxidation of the substrate is controlled simply by the linear volatilization rate. The silica scale reaches a steady state thickness of approximately 10 microns for temperatures in the range of 1200°C to 1400°C (2200°F to 2550°F). This is contrasted with oxidation under dry conditions, whereby oxidation is governed by a parabolic rate process involving the formation and growth of a stable, protective silica scale on the surface of silicon carbide.

(1) $$SiC + 3H_2O_{(g)} = SiO_2 + 3H_{2(g)} + CO_{(g)}$$

(2) $$SiO_2 + H_2O_{(g)} = Si\text{-}O_x\text{-}H_{y(g)}$$

Further work by these authors modeled the volatilization process and showed that the flux of the volatile species is controlled by diffusion through a boundary layer. For a flat plate geometry and for laminar flow, the flux is predicted to be dependent on the gas velocity and pressures as shown in equation (3) for when the volatile silicon species is $Si(OH)_4$ which is the predicted dominant species for fuel lean, gas turbine combustion environments.

(3) $$J_{Si(OH)4} \propto v^{1/2} \cdot (P_{H2O})^2 / (P_{total})^{1/2}$$

where J is the flux, v is the gas velocity and P is either the total system pressure or partial pressure of steam.

Experimental work by Robinson and Smialek[5] in a high-pressure combustion test facility measured SiC recession versus test conditions and confirmed equation (3) for lean combustion conditions. Figure 1.1.1 summarizes the results for lean burn conditions over the temperature range of approximately 1200°C to 1450°C (2200°F to 2650°F). Table 1.1.1 provides predictions based on the experimental data for long-term recession of SiC in a combustion environment. The predicted recession at 1200°C (2200°F) of 270 microns in 1000 hours in a combustion environment for SiC is too significant to ignore

for a material with expected useful life 30,000 hours in a proposed application such as an industrial gas turbine. Confirmation of this behavior in actual engine environments has been observed in a Solar Turbines, Inc. Centaur 50S industrial gas turbine[6]. The Solar Turbines, Inc. engine was run with SiC CMC combustor liners at nominally 1200°C (2200°F) for 5,018 hours. Recession values of up to ~2200 microns were measured. This recession rate is roughly 0.44 microns per hour to result in a 1,000 hour calculated recession of 440 microns, which is similar to the predicted loss of 270 microns in 1,000 hours at 1200°C (2200°F) from Table 1.1.1. Figure 1.1.2 is a view of the liner in cross section at two different locations after 5,108 hours.

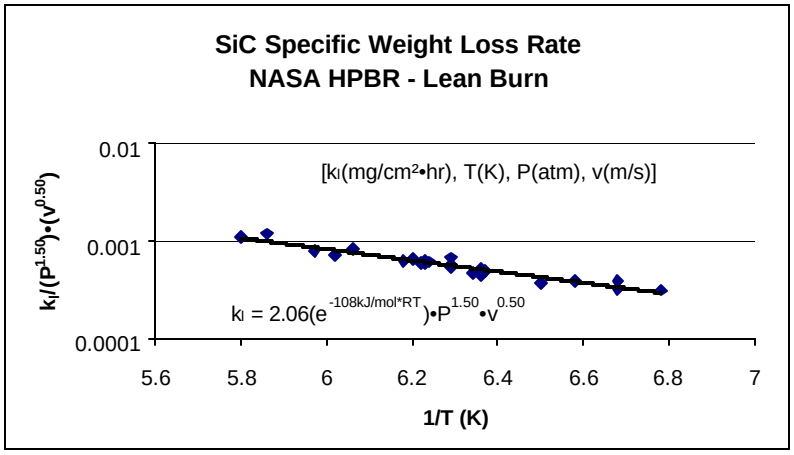

Figure1.2.1 Experimental recession measurements of SiC in a high-pressure combustion environment.

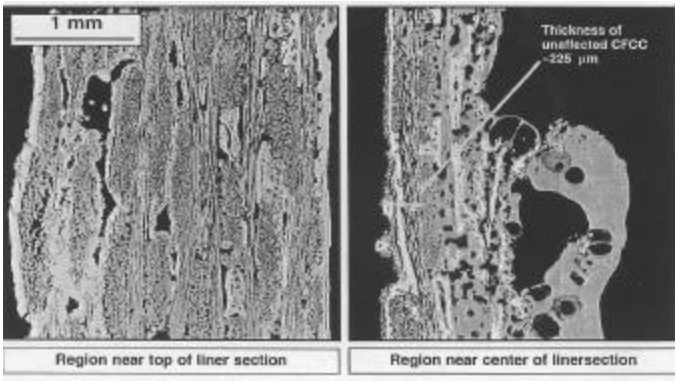

Figure1.2.2 Cross sectional view of Solar Turbines, Inc SiC CMC Centaur 50S combustor liner after 5,018 hrs operation @ nominally 1200°C showed more than 90% oxidation.

Table 1.2-1 Predicted recession of SiC under lean burn combustion conditions (Ref. 5).

T (°C)	Predicted Lean Burn Recession (μm) 1000 hrs, 10 atm, 90 m/s
1000	70
1100	140
1200	270
1300	480
1400	790
1500	1230

The current state-of-the-art 3-layer Barium Strontium Aluminum Silicate (BSAS) based EBCs have been demonstrated for more than 50,000 hours cumulative (15,144 hours continuous) at nominal 1200°C (~2200°F) in Solar Turbines Centaur 50S engine tests, under the Ceramic Stationary Gas Turbine (CSGT) and Advanced Material Program sponsored by the U.S. Department of Energy (DoE). Engine tests have been performed at three sites: Chevron Texaco Exploration and Production Inc. in Bakersfield, CA, Malden Mills Industries in Lawrence, MA and a California Dairies site in Valencia, CA. To date, eight sets of combustor liners with BSAS-based EBCs applied by UTRC have been tested. The lessons learned from these engine tests have laid the foundation for continued improvements in the EBC coatings and develop a fundamental understanding of the life limiting mechanisms. One of the key gaps in the assessment of EBCs has been the effects of the combination of stress and environmental effects (high pressure, high velocity steam) on the durability of CMCs. An attempt was made at durability assessment under the current enabling technologies program.

1.3 Durability determination of EBC Coated CMCs

The durability evaluation of uncoated and EBC-coated CMCs was done via long term exposure testing performed by Oak Ridge National Laboratory (ORNL). The ORNL rig is atmospheric with local water vapor content of up to 0.9 atm and is able to run three specimens in one furnace with independent load control. The tests were run at 2200°F, 90% steam with stress (16 ksi and 24 ksi) that was removed every eight hours for 5 minutes. The combination of stress and moisture content of the tests are designed to be more severe than those expected in typical CMC combustor applications.

MI SiC/SiC CMC specimens with EBC have survived 500 hours and 2000 hours of testing in water-vapor rich elevated temperature testing at Oak Ridge National Laboratory (ORNL). The results are presented in Table 1.2.1. The current and past results demonstrate that an EBC is essential to the long term durability of MI SIC/SiC in water vapor rich combustion environments. The current results also demonstrate that the MI SiC/SiC with an EBC retained good mechanical properties after 2000 hours of exposure.

Table 1.3-1 Long term durability test data

							Ultra-Low Cycle Fatigue			Post Exposure
Duration (hr)	**Temp. (F)**	**Humidity**	**Stress Level (ksi)**	**Applied Load - 4 Pt. (N)**	**Specimen Type**	**Specimen Number**	**Freq.**	**Unload Duration**	**R Ratio**	**Relative Flexural Strength**
0	RT				uncoated	F-5				**0.9**
					uncoated	F-6				**1.1**
					uncoated	Average				**1.0**
	2200				uncoated	F-7				**0.6**
					uncoated	F-8				**0.6**
					uncoated	Average				54.9
500	2200	90%	16	27.0	uncoated	F-1	8hr	5 min	0.1	0.1
			16	27.0	coated	FC-1	8hr	5 min	0.1	**0.7**
			24	40.5	coated	FC-2	8hr	5 min	0.1	**1.1**
2000	2200	90%	16	27.0	coated	FC-3	8hr	5 min	0.1	no data
			24	40.5	coated	FC-4	8hr	5 min	0.1	**0.7**
			24	40.5	coated	FC-5	8hr	5 min	0.1	on hold

The MI SiC/SiC material was fabricated by Goodrich Corporation using Tyranno SA fiber and a standard BN interface coating. The tensile properties measured by Goodrich on the MI SiC/SiC used in this testing are presented in Table 1.2.2 and show that the material has good mechanical properties. Flexural curves measured by Southern Research Institute at room temperature and 2200°F. Panel 521 was used for the baseline flexural testing and Panel 520 was used for the long term durability flexural testing. The microstructure of panels 520 and 521 are presented in Figures 1.2.1 and 1.2.2, respectively.

Table 1.3.2 *Tensile Data on MI SiC/SiC panels*

Test	**Conditions**	**Panel No ***	**Number of Tests**	**Strength (ksi)**	**Modulus (Msi)**	**Strain to Failure (%)**	**Proportional Limit (ksi) ****
Tensile	RT	520	T-1	47.2	36.6	0.28	27.3
			T-2	48.8	35.9	0.31	25.7
			Average	**48.0**	**36.3**	**0.30**	**26.5**
		521	T-2	55.7	34.5	0.36	24.3
		520 & 521	**Average**	**50.6**	**35.7**	**0.32**	**25.8**
ILT	RT	520	ILT-1	2.14			
			ILT-2	2.32			
			ILT-3	2.82			
			Average	2.43			
		521	ILT-1	2.70			
			ILT-2	3.02			
			ILT-3	2.81			
			Average	2.84			
		520 & 521	**Average**	**2.64**			

* Fiber v/o: 520 - 38%, 521 - 41%

** 0.005% offset

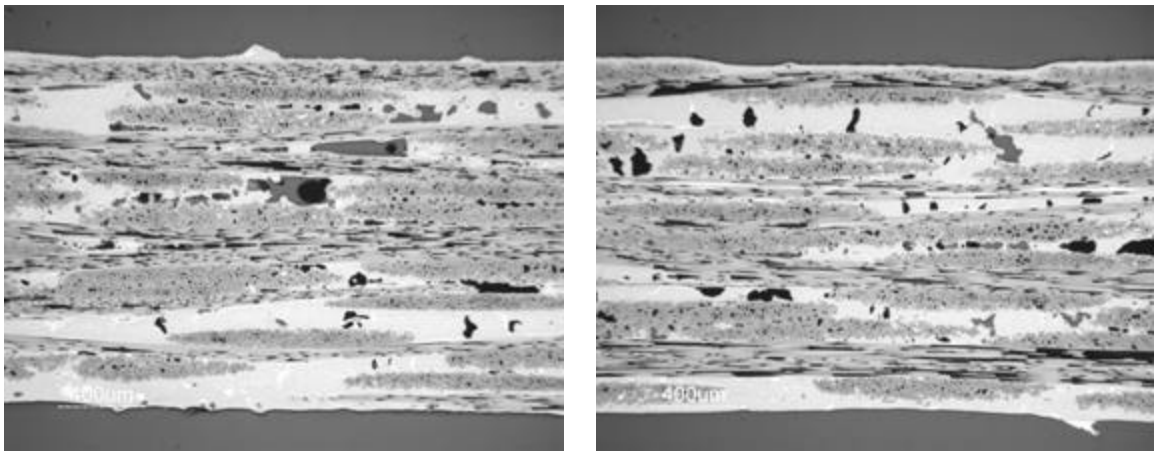

Figure 1.3.1 Microstructure of panel 520.

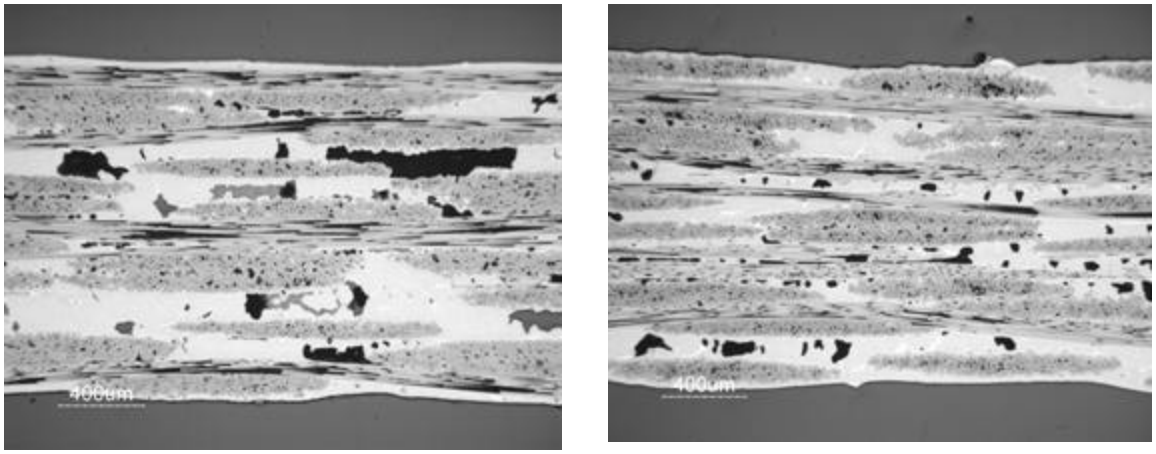

Figure 1.3.2 Microstructure of panel 521.

Flexure samples with a 0.090” diameter hole was EBC coated using a three layer Strontium aluminosilicate (SAS), mullite, silicon coating applied by air plasma spray. The front and back of the coated specimens are shown in Figure 1.2.3. It was difficult to obtain good, uniform coating on the edges and inside the 0.090” diameter hole.

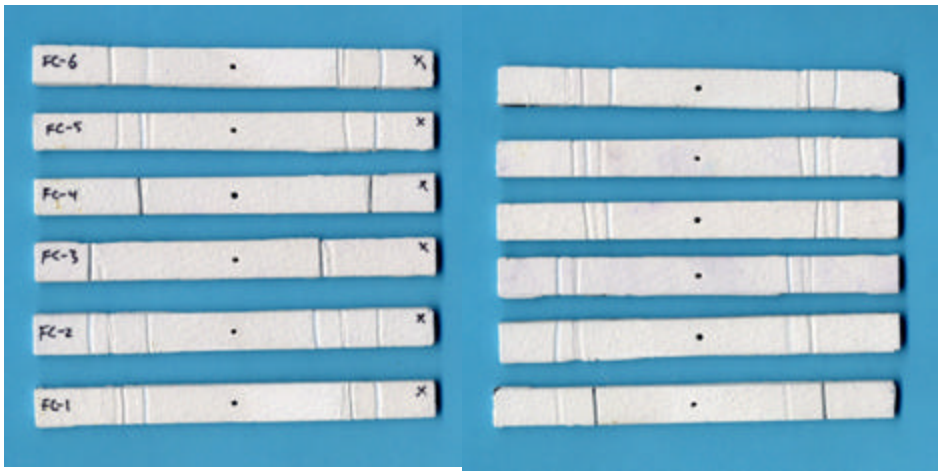

Figure 1.3.3 EBC coated long term durability specimens

500 and 2000 Hour Exposure Tests

The 500 hour exposure clearly demonstrated the necessity of the EBC in an elevated temperature moisture environment (Table 1.2.1). The residual flexural strength retention of the uncoated specimen was < 10% of baseline compared to 70-100% for the coated specimen (FC-2) exposed at 2200°F, 90% humidity, for both stress levels studied. The retention of good mechanical properties was also demonstrated during the 2000 hour exposure. Coated specimen (FC-4) had a residual flexural strength retention of ~70% after being exposed at 2200°F, 90% humidity, 24 ksi. However, CT scans (Figure 1.2.4) of the samples and visual examinations show evidence of coating deterioration and delaminations around the holes. Despite the CMC deterioration over time, the good mechanical properties were retained and the broader implications of this result have yet to be established.

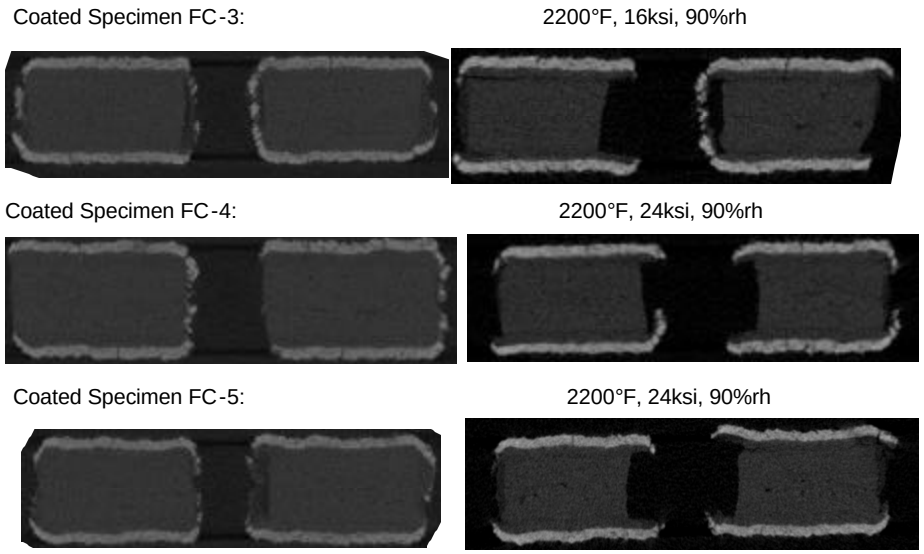

a) as-received b) after exposure

Figure 1.3.4 CT scan of 0.090" dia. hole region before and after 2000 hour exposure. Note: cross-section may not be at the center of the hole.

2.0 Design and Testing of Ceramic Components

2.1 Introduction

Ceramic Matrix Composites (CMCs) are considered an enabling turbine engine material because of their high thermal-mechanical performance and low density compared to metal alloy and intermetallic materials. Furthermore, CMCs have demonstrated improvements in apparent toughness and failure strain compared to monolithic ceramic materials[7]. The introduction of CMC combustor liners in industrial gas turbines (IGTs) with premixed combustors has resulted in reduced emissions and higher cycle efficiency[8,9]. CMC turbine vanes have also been designed and rig tested in representative environments[9,10]. More recently, CMC combustor liners have been demonstrated to lower CO and NO_x emissions in a Pratt & Whitney FT8 sector rig[11,12] The combustor liner for the FT8 engine incorporates a straight cylinder can-annular design. The primary thrust of the current activity was to demonstrate the performance benefits of a full annular reverse flow CMC combustor in an aero-engine type environment.

Reverse flow full annular combustors are commonly used throughout many of P&W's small gas turbine engines. Gas turbine engines with reverse flow combustors are used in some helicopters and small business jets. A standard metal combustor design for PW200 series engines is illustrated in Figure 2.1.1 The metal combustor has rows of small holes for film cooling of the metal combustor to prevent it from overheating.

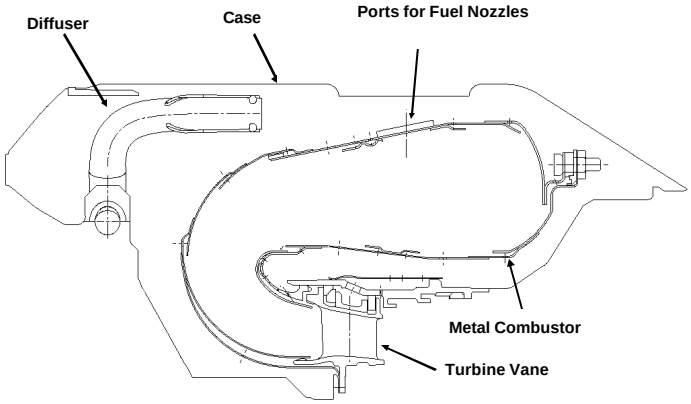

Figure 2.1.1 Standard metal combustor design for PW200 series engines

The CMC combustor offers the potential elimination of the film cooling to provide reduced emissions and increased durability. The high temperature capability of the CMC is expected to increase the life of the combustor components while enabling the elimination of film cooling and a reduction of combustor cooling. The engine will be more efficient since less combustor wall cooling is required (up to ~70% reduction in cooling). In addition, the profile of the combustion gas entering the turbine is predicted to improve which is expected to increase the life of turbine components. Further improvements in the CO, NO_x and smoke emissions are projected. UTRC's PW206 gas generator rig was modified to a combustor rig and an advanced combustor concept was

demonstrated through the measurement of improved pattern factor and reduced emissions over baseline.

2.2 Design of Advanced CMC Combustor

One of the key challenges in designing with the ceramic components is developing an attachment methodology that minimizes the high thermal stresses that are generated due to thermal expansion mismatch between the low CTE ceramics and high CTE metallic components. In addition to the CTE mismatch induced thermal stresses, the CMC combustor is also subject to high mechanical loads due to differences in the internal and external pressures on the liner.

In order to optimize performance and reduce the thermal expansion differences between CMC liners and metal shells, the advanced PW206 with CMC combustor had a modified fuel system with axial fuel nozzles as opposed to the baseline that had radial fuel nozzles. Extensive CFD analysis was conducted to predict the performance of the advanced combustor and provide the boundary conditions for detailed design and structural analysis.

The advanced combustor consists of three-piece CMC liners in metallic shells which are designed to be regenerative cooled, i.e. cooling air is not injected as a film but instead is injected with the dilution hole flow. This combustor design is enabled by CMCs and is predicted to have a much improved pattern factor and reduced emissions. The improved mixing and reduced film cooling is shown in the results from the CFD analysis is depicted in Figure 2.2.1

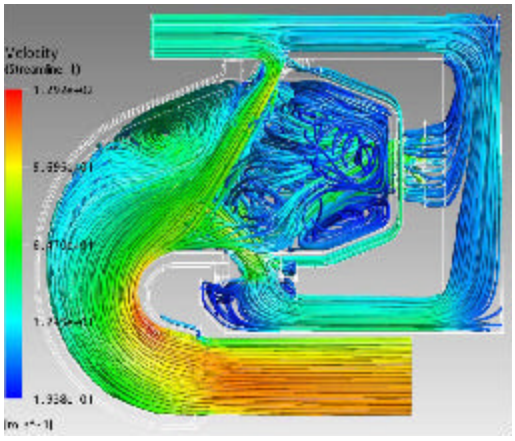

Figure 2.2.1 Gas velocity from CFD analysis that depicts improved mixing at combustor exit

In the conceptual design phase, special attention was paid to attaching the CMC combustor liner to a metal support so that thermal stress due to differential thermal growth between the metal support and the CMC combustor liner is minimized. Several attachment concepts were generated and a final down-select was made based on the ease

of manufacturing, attachment stress, leakage control, effect on combustion process, emissions benefit, and production cost.

The basic design features of the advanced PW206 CMC reverse flow combustor are shown in Figure 2.2.2. The CMC liner is composed of a dome, large entry duct (LED) and small entry duct (SED) shown in Figures 2.2.3. These CMC components interface with inner and outer metal air inlet rings. The assembly is held together by a metal support shell that is connected to the air inlet rings. Figure 2.2.4 shows a schematic of the arrangement. The external metallic shell is made of sheet metal and the pieces are formed to support the CMC shell that is held in a compressive state. Additionally, two annular metallic rings complete the combustor assembly. The metallic skins are designed to compress the CMC shells against the metal air inlet rings. The metal skins are then welded to the ring, thus trapping the CMC shell in compression through metallic springs located between the shells. Much of the air required for combustion is admitted through holes in the metal rings and the nozzles.

This design allows the thermal expansion mismatch between the combustor and the engine case to be accommodated. The CMC shells are isolated from the cold metal shell deformations by the metallic springs which absorb the mismatch in expansion.

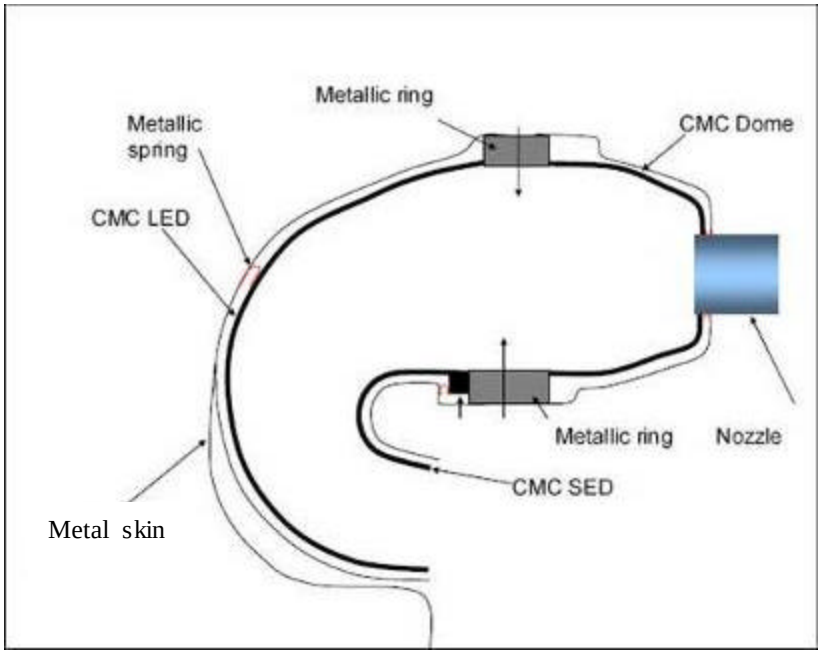

Figure 2.2.2 Basic Design Features of Advanced CMC combustor

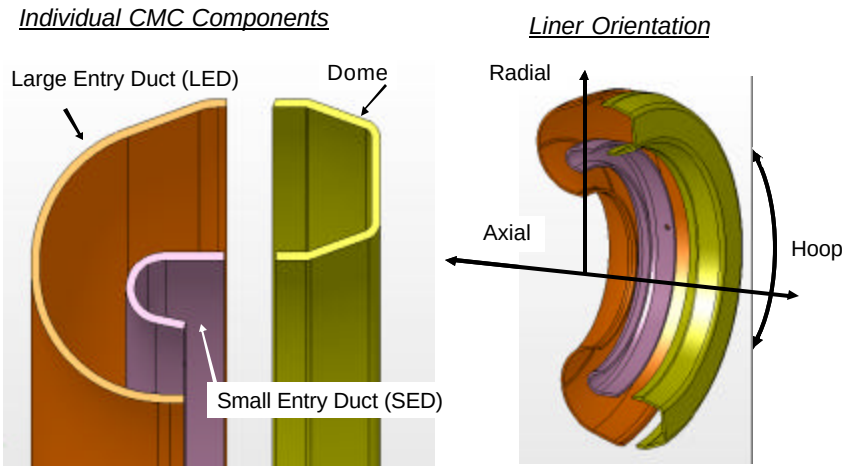

Figure 2.2.3 CMC components for a CMC reverse flow combustor

The detailed steps in the detailed thermostructural analysis of the CMC combustor is illustrated in Figure 2.2.4

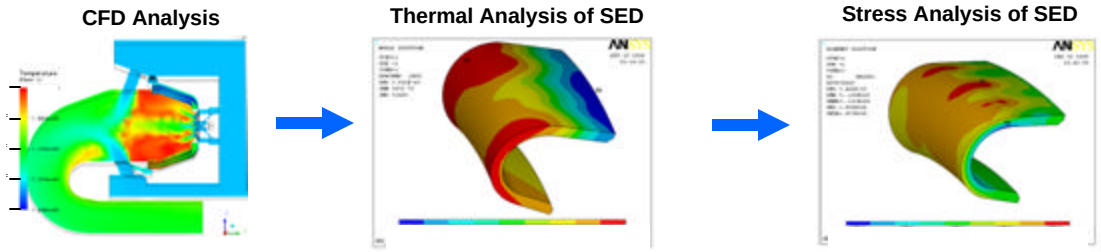

Figure 2.2.4 Analysis sequence applied to PW206 CMC combustor

The results of thermal analysis presented in Figures 2.2.4 show that the maximum temperature on the CMC are well within the average capability for MI SiC/SiC. The subsequent stress analysis also found that the stresses in PW206 CMC components do not exceed the material's average capability.

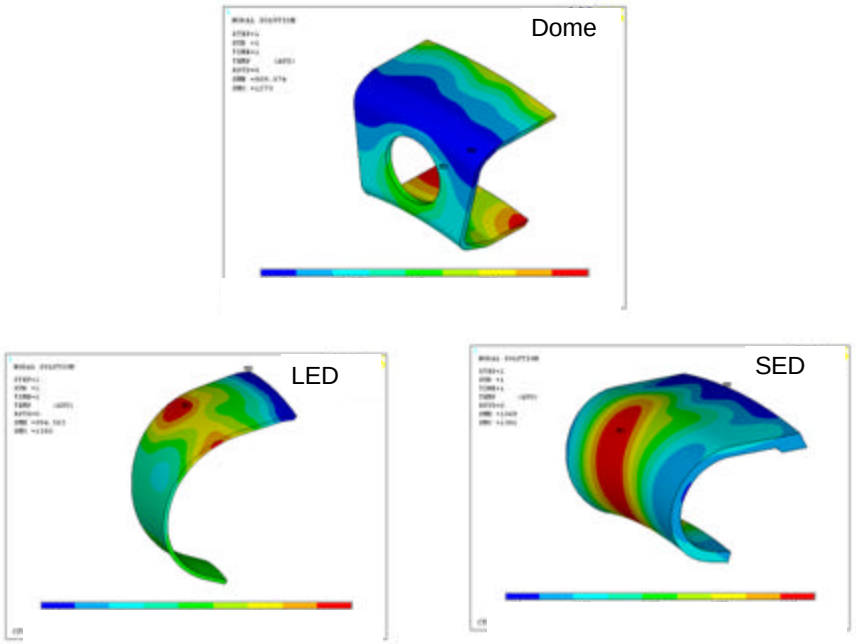

Figure 2.2.5 Thermal analysis of CMC components showing that the predicted temperatures do not exceed the temperature capability of the material

2.3 Fabrication

After extensive fiber architecture analyses, a pseudo 0/90 lay-up was selected for the three CMC components. UBE's Tyranno SA fiber was down selected for this application. Goodrich fabricated the CMCs component with the fiber perform weaving being subcontracted to Albany Engineered Composites (AEC). Goodrich consolidated the woven performs by the following process: BN interface and SiC matrix deposition by chemical vapor infiltration (CVI), SiC particulate infiltration by aquious slurry cast and final consolidation by Si melt infiltration (MI). The resultant CMC was a melt infiltrated composite (MI SiC/SiC). The fully consolidated test articles were machined by diamond grinding to final dimensions. The SED and LED were seal coated by Goodrich after they went through machining to enhance oxidative stability. Due to schedule considerations, the dome was not seal coated.

The components were subsequently coated by a Environmental Barrier Coating (EBC). As described in chapter 1, the EBC is critical for protection of the CMC against high pressure, high velocity water vapor rich combustion environments. The EBC for the CMC components consisted of a silicon (Si) bond coat and a yttrium silicate (YS) top coat. The processing of the EBC had to be scaled up to coat the components. EBC coated CMC components are shown in Figure 2.3.1.

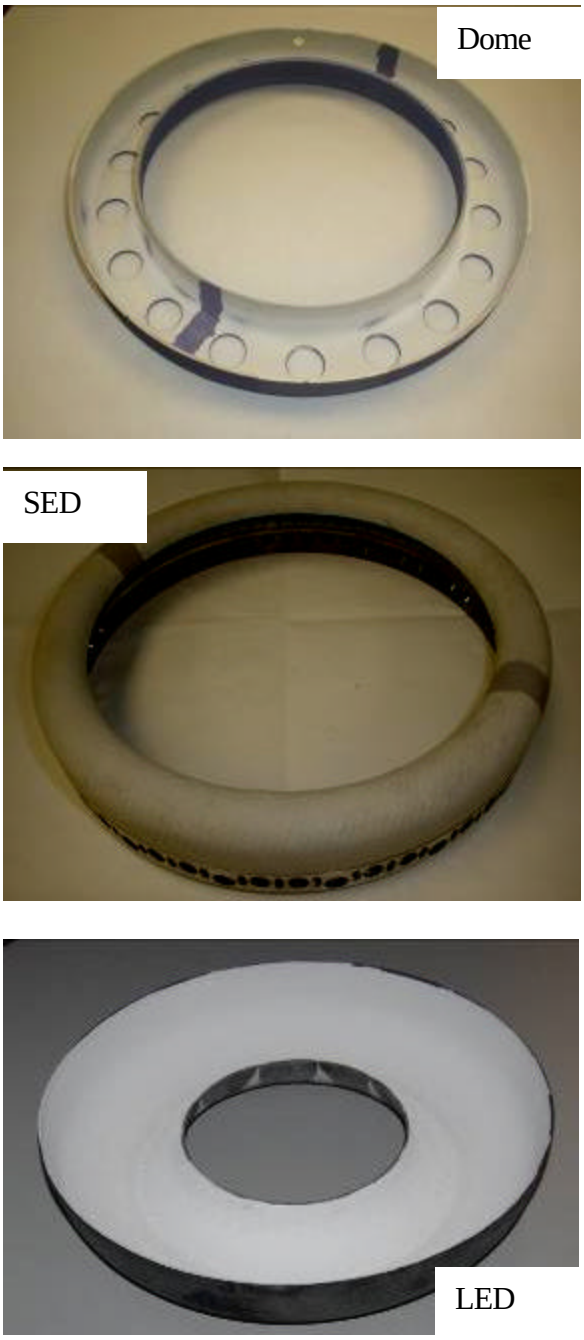

Figure 2.3.1 EBC Coated CMC Components

2.4 Assembly of Advanced CMC Combustor in PW206 rig

The PW206 CMC combustor was assembled to ensure that the stack up and welding specifications laid out in the procedure were met. Prior to assembly, the EBC coated CMC dome, SED and LED were thermal painted, and inspected using white light to insure dimensional accuracy. The assembled combustor was instrumented and assembled into the combustor rig for test. A fully assembled CMC combustor is shown in Figure 2.4.1.

Figure 2.4.1 Fully Assembled Advanced CMC Combustor

2.5 Combustor Rig Testing and Performance

In order to measure and quantify the performance of the CMC combustor, measurements of radial temperature variations, pattern factor and emissions had to be made. A custom rotating temperature rake consisting of 10 thermocouples at varying radial locations was designed, fabricated and used to measure temperature at the combustor exit duct. Figure 2.5.1 shows the temperature rake and an assembled PW206 combustor rig.

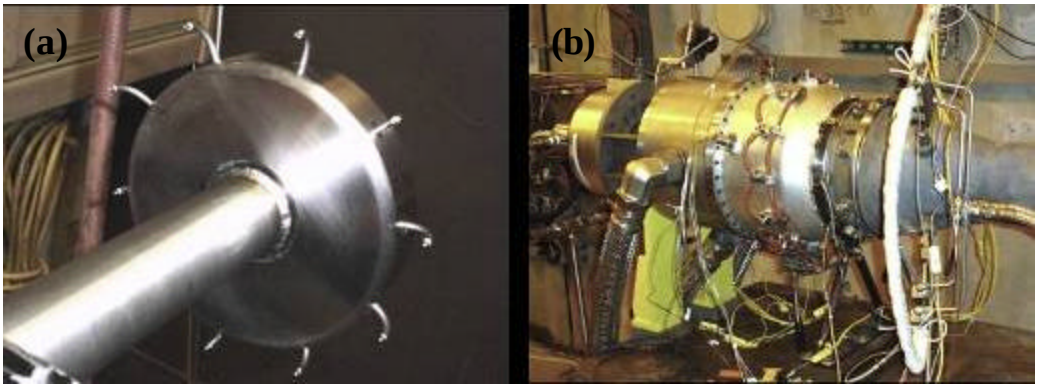

Figure 2.5.1 (a) Custom temperature probe (b) PW206 combustor rig.

In preparation for a combustor rig test, a baseline metal rig test was performed to reduce risks associated with assembly and testing. The metal combustor rig test was performed and all thermocouples survived test to a simulated 100% power condition. The radial temperature profile was measured and was found to be in the range expected for a PW206. The pattern factor was also measured to lie within the range expected from the metal PW206 combustor.

The advanced PW206 CMC combustor including the CMC hardware, metal hardware and the fuel system was successfully rig tested. The combustor ran to 100% power on two occasions and survived three unplanned trip shutdowns. All thermocouples survived test to a simulated 100% power condition. Data was collected for all the design points

planned. The pattern factor was reduced by over 40% of baseline and surpassed the goals of the program. The NO_x emission index was reduced by approximately 30% over the baseline. Significant improvement was not observed in CO emissions and the reasons for that are not obvious at this time. Figure 2.5.2 represents contours of pattern factor exceeding a maximum threshold at measured at 100% power. It shows the dramatic improvement over baseline and demonstrates the much greater temperature uniformity in the CMC combustor. The pattern factor and NOx improvements validated the models that predicted the performance. Figure 2.5.3 shows the picture of the combustor after the test and more detailed visual inspection shows the combustor to be in good condition.

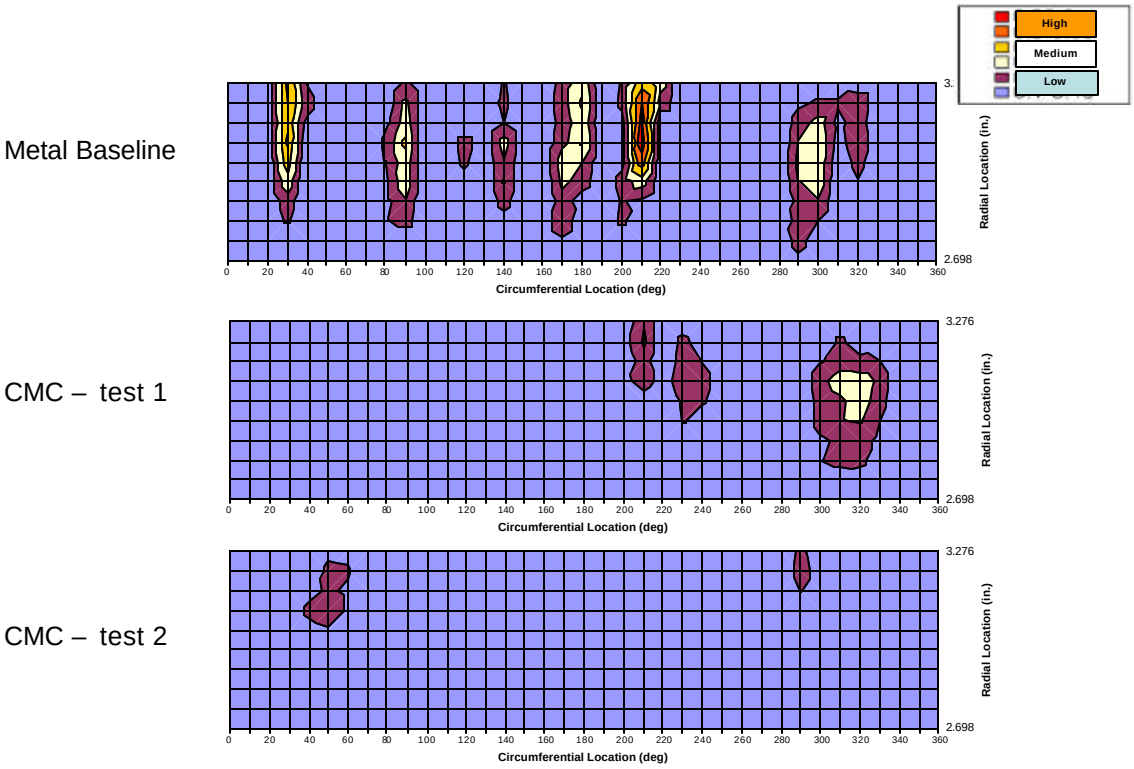

Figure 2.5.2 Measured Pattern Factor at Combustor Exit at 100% Max power as a function of span.

Figure 2.5.3 Advanced CMC combustor after rig test.

3.0 Summary

The objective of this contract was to develop technologies critical for ceramic hot section components for gas turbine engines. Significant technical progress has been made towards incorporation of EBC and CMC technologies into gas turbine engine hot-section. The focus has been on the demonstration of a reverse flow annular CMC combustor. This has included overcoming the challenges of design and fabrication of CMCs into "complex" shapes, developing processing to apply EBCs to "engine hardware", testing of an advanced combustor enabled by CMCs in a PW206 rig and the validation of performance benefits against a metal baseline. The rig test validated many of the pretest predictions with a 40-50% reduction in pattern factor compared to the baseline and ~ 30% reduction in NOx levels at max power conditions. The next steps are to develop an understanding of the life limiting mechanisms in EBC and CMC materials, developing a design system for EBC coated CMCs, and durability testing in an engine environment.

References

1. "Oxidation of Silicon Carbide Refractory Materials", A.C. Lea, J. Soc. Glass Technology, 33 [150] 27-50T (1949); Ceram. Abstr., 1951, Novemebr, p. 198f.

2. "Paralinear Oxidation of CVD SiC in Water Vapor", E.J. Opila and R.E. Hann Jr, J. Am. Ceram. Soc., 80 (1), p. 197-205 (1997).

3. "Mass Spectrometric Identification of Si-O-OH(g) Species from the Reaction of Silica with Water Vapor at Atmospheric Pressure", E.J. Opila, D.S. Fox, and N.S. Jacobson, J. Am. Ceram. Soc., 80 (4), p. 1009-12 (1997).

4. "SiC Recession Caused by SiO_2 Scale Volatility under Combustion Conditions: II, Thermodynamcis and Gaseous-Diffusion Model", E.J. Opila, J.L. Smialek, R.C. Robinson, D.S. Fox, and N.S. Jacobson, J. Am. Ceram. Soc., 82 (7), p. 1826-34 (1999).

5. "SiC Recession Caused by SiO_2 Scale Volatility under Combustion Conditions: I, Experimental Results and Empirical Model", R.C. Robinson and J.L. Smialek, J. Am. Ceram. Soc., 82 (7), p. 1817-25 (1999).

6. "EBC Protection of SiC/SiC Composites in the Gas Turbine Combustion Environment", H.E. Eaton, G.D. Linsey, K.L. More, J.B. Kimmel, J.R. Price, and N. Miriyala, ASME 2000-GT-631, Munich 2000.

7. "Ceramic Gas Turbine Design and Test Experience", M. van Roode, M.K. Ferber, and D. Richerson, Progress in Ceramic Gas Turbine Development, Vol. 1, Eds, ASME Press, New York, 2002.

8. "The Evaluation of CFCC Liners After Field Testing in a Gas Turbine – IV", J. Kimmel, J. Price, K. More, P. Tortorelli, E. Sun, and G. Linsey, Proceedings of Turbo Expo 2003, Power for Land, Sea, and Air, June 16-19, Atlanta, Georgia, ASME Paper GT2003-38920.

9. "Ceramic Matrix Composite Vane Subelement Testing in a Gas Turbine Environment", M. Verrilli, A. Calamino, R.C. Robinson, and D.J. Thomas, Proceedings of ASME Turbo Expo 2004, Power for Land, Sea, and Air, June 14-17, 2004, Vienna, ASME Paper GT2004-53970.

10. "Ceramic Matrix Composite Vanes for Gas Turbine Engines", V. Vedula, J. Shi, D. Jarmon, S. Ochs, L. Oni, T. Lawton, K. Green, L. Prill, J. Schaff, and G. Linsey, Proceedings of ASME Turbo Expo 2005, Power for Land, Sea, and Air, June 6-9, 2005, Reno, Nevada, ASME Paper GT2005-68229

11. "Ceramic Matrix Composite Vanes for Gas Turbine Engines", V. Vedula, J. Shi, D. Jarmon, S. Ochs, L. Oni, T. Lawton, K. Green, L. Prill, J. Schaff, and G. Linsey, Proceedings of ASME Turbo Expo 2005, Power for Land, Sea, and Air, June 6-9, 2005, Reno, Nevada, ASME Paper GT2005-68229.

12. Final Report ONR contract N00014-06-C-0477.

Acknowledgements

This work and the efforts leading to it would not have been possible without the guidance and support of the Office of Naval Research (ONR) [Dr. David Shifler] and the Department of Energy (DoE) Distributed Energy (Office of Electricity) [Deborah Haught and Don Geiling]. The cost sharing provided by the United Technologies Corporation is gratefully acknowledged. In addition, many other UTRC, ORNL and Pratt & Whitney personnel helped make this project a success including the following:

UTRC
Marilyn Arno
Tania Bhatia
David Bombara
Shaoluo Butler
John Holowczak
David Jarmon
Scott Kearney
Gary Linsey
Robert Parker Jr.
Russ Plouard
Jun Shi
Bill Tredway
Jodi Vecchiarelli
Venkat Vedula
Jeffery Walker
Mike Weber
Jim Wilkinson
Roy Wong
Joe Wysocki

Pratt & Whitney
Robert Van Amelsvoort
Doug Berczik
Fredrick Berube
John Hu,
Matt Kennedy
Emmanuel Landriault
Joel Larose
Alex Prociw
Aleksandar Kojovic
Saeid Oskooei
Kevin Rugg
Robert Sze

Oak Ridge National Laboratories
H.T.Lin